Genomic Instability and Pro-Tumoral Inflammation are associated with Primary Resistance to Anti-PD1 + Anti-Angiogenesis in Malignant Pleural Mesothelioma

Francois-Xavier Danlos, Matthieu Texier, Bastien Job, Severine Mouraud, Lydie Cassard, Capucine Baldini, Andrea Varga, Andrey Yurchenko, Audrey Rabeau, Stephane Champiat, et al.

RESEARCH ARTICLE

Genomic Instability and Protumoral Inflammation Are Associated with Primary Resistance to Anti–PD-1 + Antiangiogenesis in Malignant Pleural Mesothelioma

François-Xavier Danlos[1,2,3], Matthieu Texier[4], Bastien Job[5], Severine Mouraud[2], Lydie Cassard[6], Capucine Baldini[1], Andrea Varga[1], Andrey A. Yurchenko[7], Audrey Rabeau[8], Stéphane Champiat[1,2], Diane Letourneur[2,9], Delphine Bredel[2], Sandrine Susini[2], Yuna Blum[10], Aurelien Parpaleix[11], Cedric Parlavecchio[11], Lambros Tselikas[2,3,12], Jean-Eudes Fahrner[2], Anne-Gaelle Goubet[2,3], Mathieu Rouanne[2,3], Saloomeh Rafie[1], Alae Abbassi[1], Ines Kasraoui[13], Marie Breckler[14], Siham Farhane[1], Samy Ammari[13], Salim Laghouati[15], Anas Gazzah[1], Ludovic Lacroix[16], Benjamin Besse[17], Nathalie Droin[14], Marc Deloger[5], Sophie Cotteret[18], Julien Adam[19], Laurence Zitvogel[2,3], Sergey I. Nikolaev[7], Nathalie Chaput[6,20], Christophe Massard[1], Jean-Charles Soria[21], Carlos Gomez-Roca[8], Gerard Zalcman[22], David Planchard[17], and Aurelien Marabelle[1,2,3]

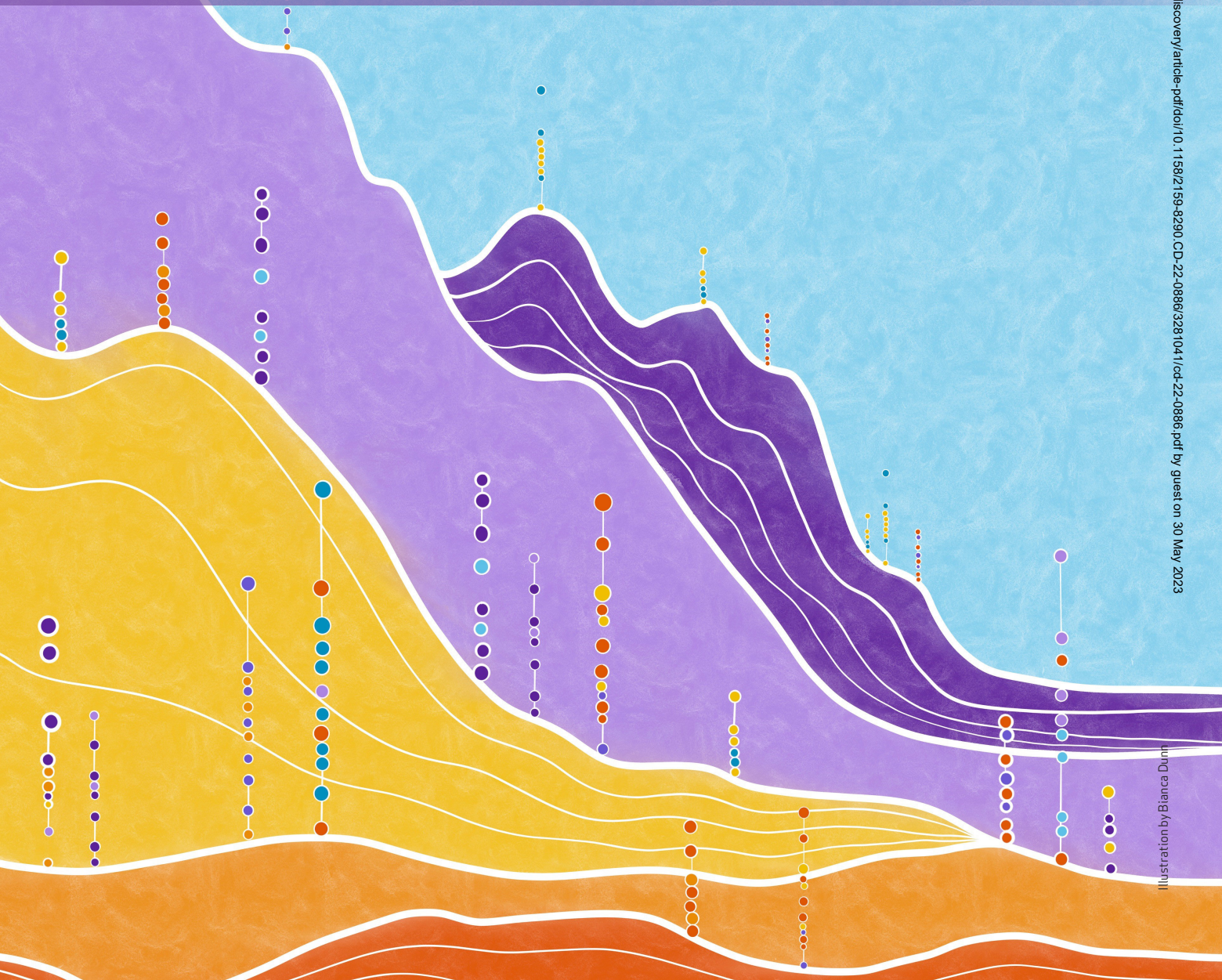

Illustration by Bianca Dunn

ABSTRACT Cancer immunotherapy combinations have recently been shown to improve the overall survival of advanced mesotheliomas, especially for patients responding to those treatments. We aimed to characterize the biological correlates of malignant pleural mesotheliomas' primary resistance to immunotherapy and antiangiogenics by testing the combination of pembrolizumab, an anti–PD-1 antibody, and nintedanib, a pan-antiangiogenic tyrosine kinase inhibitor, in the multicenter PEMBIB trial (NCT02856425). Thirty patients with advanced malignant pleural mesothelioma were treated and explored. Unexpectedly, we found that refractory patients were actively recruiting $CD3^+CD8^+$ cytotoxic T cells in their tumors through CXCL9 tumor release upon treatment. However, these patients displayed high levels of somatic copy-number alterations in their tumors that correlated with high blood and tumor levels of IL6 and CXCL8. Those proinflammatory cytokines resulted in higher tumor secretion of VEGF and tumor enrichment in regulatory T cells. Advanced mesothelioma should further benefit from stratified combination therapies adapted to their tumor biology.

SIGNIFICANCE: Sequential explorations of fresh tumor biopsies demonstrated that mesothelioma resistance to anti–PD-1 + antiangiogenics is not due to a lack of tumor T-cell infiltration but rather due to adaptive immunosuppressive pathways by tumors, involving molecules (e.g., IL6, CXCL8, VEGF, and CTLA4) that are amenable to targeted therapies.

INTRODUCTION

Unresectable malignant mesothelioma (MM) is a cancer developed from pleural and peritoneal serous membrane linings upon chronic exposure to environmental silicate minerals such as asbestos (1). Indeed, chronic exposure of serous membranes to asbestos microparticles leads to inflammation, recruitment of inflammatory macrophages, development of an immunosuppressive protumoral microenvironment, constitution of pathologic neoangiogenesis with hypoxia, and eventually serous cells' malignant transformation toward an aggressive phenotype leading to metastatic disease (2, 3). Advanced MMs are incurable cancers with a historical median overall survival typically around 12 months with platinum doublet chemotherapies (4) but slightly better for epithelioid than nonepithelioid (biphasic and sarcomatoid) histotypes (5). Targeting the tumor microenvironment (TME) with immune-checkpoint blockers or antiangiogenic drugs has recently shown significant activity in several metastatic cancers. Angiogenesis contributes to tumor growth and the development of metastases, but the modulation of neoangiogenesis via inhibition of the VEGF/VEGFR pathway has shown antitumor activity in several human solid cancers (6). Also, blocking immune checkpoints with antagonistic monoclonal antibodies targeting programmed death-1 receptor (PD-1) and its ligand (PD-L1) has been extensively investigated in the recent past and is still in active development across malignancies (7). Combining antiangiogenic drugs and anti–PD-(L)1 antibodies has recently shown important synergistic results in renal cell carcinoma, hepatocellular carcinoma, and non–small cell lung cancer (NSCLC; refs. 8–10). Indeed, anti-VEGF therapies may enhance anti–PD-1/PD-L1 efficacy by reversing

[1]Département d'Innovation Thérapeutique et d'Essais Précoces (DITEP), Gustave Roussy, Villejuif, France. [2]INSERM U1015 and CIC1428 BIOTHERIS, Gustave Roussy, Villejuif, France. [3]Faculté de Médecine, Université Paris-Saclay, Kremlin-Bicetre, France. [4]Service de Biostatistique et d'Épidémiologie, Oncostat INSERM U1018, Gustave Roussy, Université Paris-Saclay, Villejuif, France. [5]Plateforme de Bioinformatique, Université Paris-Saclay, INSERM US23, CNRS-UMS 3655, Gustave Roussy, Villejuif, France. [6]Laboratoire d'Immuno-Oncologie (LIO), CNRS-UMS 3655 and INSERM US23, Gustave Roussy, Villejuif, France. [7]INSERM U981, Gustave Roussy, Université Paris-Saclay, Villejuif, France. [8]Department of Medical Oncology, Institut Claudius Regaud, Institut Universitaire du Cancer de Toulouse, Toulouse, France. [9]École Normale Supérieure de Lyon, Université Claude Bernard Lyon I, Université de Lyon, Lyon, France. [10]Institut de Génétique et Développement de Rennes (IGDR), UMR6290 ERL U1305 CNRS, INSERM, Université de Rennes, Rennes, France. [11]Equipe Promotion – Bureau Projets et Promotion (BPP) – Direction de la Recherche Clinique (DRC), Gustave Roussy, Villejuif, France. [12]Département d'Anesthésie, Chirurgie et Imagerie Interventionnelle (DACII), Gustave Roussy, Villejuif, France. [13]Département de Radiologie, Biomaps, UMR1281 INSERM, CEA, CNRS, Gustave Roussy, Université Paris-Saclay, Villejuif, France. [14]INSERM US23, CNRS UAR 3655, AMMICa, Genomic Platform, Gustave Roussy Cancer Center, Villejuif, France. [15]Unité Fonctionnelle de Pharmacovigilance, Gustave Roussy, Villejuif, France. [16]Département de Biologie et Pathologie médicales, Plateforme de Biopathologie Moléculaire, CNRS-UMS 3655 and INSERM US23, Villejuif, France. [17]Département de Médecine Oncologique, Gustave Roussy, Villejuif, France. [18]Laboratoire de Cytogénétique, Gustave Roussy, Villejuif, France. [19]INSERM U1186, Gustave Roussy, Villejuif, France. [20]Faculté de Pharmacie, Université Paris-Saclay, Orsay, France. [21]Amgen, Thousand Oaks, California. [22]Service de Pneumologie, Hopital Bichat, APHP, Université de Paris, Paris, France.

Corresponding Authors: Aurelien Marabelle, Département d'Innovations Thérapeutiques et d'Essais Précoces (DITEP), 114 Rue Edouard Vaillant, 94805 Villejuif, France. Phone: 331-4211-5592; E-mail: aurelien.marabelle@gustaveroussy.fr; and François-Xavier Danlos, Département d'Innovations Thérapeutiques et d'Essais Précoces (DITEP), 114 Rue Edouard Vaillant, 94805 Villejuif, France. Phone: 331-4211-6350; E-mail: francois-xavier.danlos@gustaveroussy.fr

Cancer Discov 2023;13:1–22

doi: 10.1158/2159-8290.CD-22-0886

VEGF-mediated immunosuppression and promoting T-cell infiltration in tumors (11). Recently, translational studies have illustrated that PD-1/PD-L1 and angiogenesis pathways are involved in MM tumors and could better characterize the biology of those tumors than the historical histotypes (12). Both antiangiogenic and immune-checkpoint blockers have indeed shown activity in advanced pleural mesothelioma. Bevacizumab, an IgG1 monoclonal antibody targeting VEGFA, in association with platinum-based regimen chemotherapy, has been shown to increase the overall survival of patients with untreated unresectable pleural mesothelioma compared with chemotherapy alone (13). Nintedanib, an oral triple receptor tyrosine kinase inhibitor (TKI) of PDGFRα/β, FGFR1–3, and VEGFR1–3, has shown significant activity in combination with chemotherapy for the treatment of pleural MM in a randomized phase II trial (14), but this result could not be confirmed in a subsequent phase III trial (15). Pembrolizumab, an IgG4 monoclonal anti–PD-1 antibody, has shown limited activity in monotherapy for advanced mesothelioma, with an objective response rate (ORR) of 8% (16). More recently, the combination of an anti–PD-L1 (atezolizumab) with an anti-VEGF (bevacizumab) exhibited significant synergistic activity, with an ORR of 40% and a median duration or response of 12.8 months in peritoneal mesothelioma (17).

To date, the combination of anti–PD-1 (nivolumab) + anti-CTLA4 (ipilimumab) antibodies has been demonstrated to significantly improve the overall survival (OS) of MM patients with untreated unresectable pleural mesothelioma compared with standard-of-care chemotherapy (18). This combined immunotherapy had an ORR comparable with chemotherapy (~40%) in both epithelioid and nonepithelioid histotypes. Chemotherapy was known to provide better outcomes in epithelioid rather than sarcomatoid mesotheliomas (5). Interestingly, mesothelioma histology does not affect the efficacy of an anti–PD-1 and anti-CTLA4 combination (18). Therefore, the biggest OS benefit of anti–PD-1 and anti-CTLA4 in comparison with chemotherapy is for sarcomatoid mesothelioma. The median duration of response was longer for immunotherapy (11 months) than for chemotherapy (6.7 months), which translated into a significant benefit in OS (median OS of 18.1 vs. 14.1 months).

Therefore, it has become clear that immune-checkpoint targeted immunotherapies mostly benefit patients with MM who are responding to such treatments and that therapeutic improvements are needed for the majority of patients who are not benefiting from them. However, little is currently known about the biology of MM tumors presenting with primary resistance to anti–PD-(L)1–based therapies. In the above-mentioned nivolumab + ipilimumab trial, a slight decrease in efficacy was found when MM tumor cells did not express PD-L1 [<1% PD-L1 expression by 28–8 IHC staining on formalin-fixed, paraffin-embedded (FFPE) samples; ref. 18]. The ancillary analysis of the above-mentioned atezolizumab + bevacizumab trial could not identify significant biomarkers of activity besides an epithelial-to-mesenchymal (EMT) gene expression signature in tumors not responding to the combination therapy (17). Of note, the ETOP Beat Meso trial is an ongoing multicenter, randomized phase III study currently testing the value of adding an anti–PD-L1 (atezolizumab) to a combination of anti-VEGF (bevacizumab) and standard chemotherapy (NCT03762018). This trial follows the good results obtained by the two phase II trials, DREAM (ACTRN12616001170415) and PrE0505 (NCT02899195), testing an anti–PD-L1 (durvalumab) in combination with cisplatin and pemetrexed, with response rates of 46% and 56%, respectively, in first-line advanced pleural mesothelioma (19, 20).

Here, we report the safety and efficacy of nintedanib, a pan-antiangiogenic TKI, in combination with pembrolizumab, an IgG4 monoclonal anti–PD-1 antibody, in patients with advanced mesothelioma naive to immunotherapy and previously treated with at least one line of a platinum-based chemotherapy regimen (PEMBIB trial; NCT02856425). In this trial, we aimed to better describe the biological correlates of primary resistance to anti–PD-1 + antiangiogenics in patients with pleural MM. We performed an extensive exploration of blood and tumor samples at baseline and on treatment, including the analysis of fresh blood and fresh tumor samples by flow cytometry and by titration of cytokines, chemokines, VEGF, and soluble factors released by those fresh tissues. Our findings on fresh MM tissue, as well as fixed/frozen tissues, highlighted novel mechanisms of immunotherapy resistance, providing the rationale for novel biology-driven immunotherapy strategies in pleural MM.

RESULTS

Trial Design and Patient Characteristics

The PEMBIB trial is a multicenter phase Ib trial that consisted of a dose-escalation part to determine the recommended dose of nintedanib to be used with pembrolizumab followed by expansion cohorts in disease-specific indications. Patients treated in the expansion cohorts received nintedanib at 150 mg orally twice a day (b.i.d.) in combination with pembrolizumab at 200 mg i.v. every 3 weeks (Q3W; Fig. 1A). A nintedanib monotherapy lead-in was initiated 7 days (D −7) before initiating pembrolizumab at C1D1 (Fig. 1B). Here, we report the results of the first expansion cohort completed with patients having advanced pleural MM. Thirty-two patients were enrolled between October 10, 2017, and April 11, 2019, in the mesothelioma expansion cohort of the trial. Two patients were screen failed

Figure 1. Trial design, treatment efficacy, and outcome of the PEMBIB mesothelioma cohort. Graphical representation of treatment doses provided (**A**) and the treatment regimen (**B**) according to the PEMBIB protocol, with the blood and tumor sampling scheme. **C,** Waterfall plot depicting the best objective response on target lesions according to RECIST version 1.1 (RECIST 1.1) criteria. B, biphasic; E, epithelioid; S, sarcomatoid. **D,** Spider plot of the sum of target lesions upon treatment. **E,** Swimmer plot illustrating the individual response and clinical benefit status according to tumor histology. Durable clinical benefit (DCB) is defined as being in complete or partial response or stable disease at 6 months per RECIST 1.1 criteria. NE, not evaluable. **F,** Kaplan–Meier survival curves depicting the OS of the patients treated according to their DCB status at 6 months.

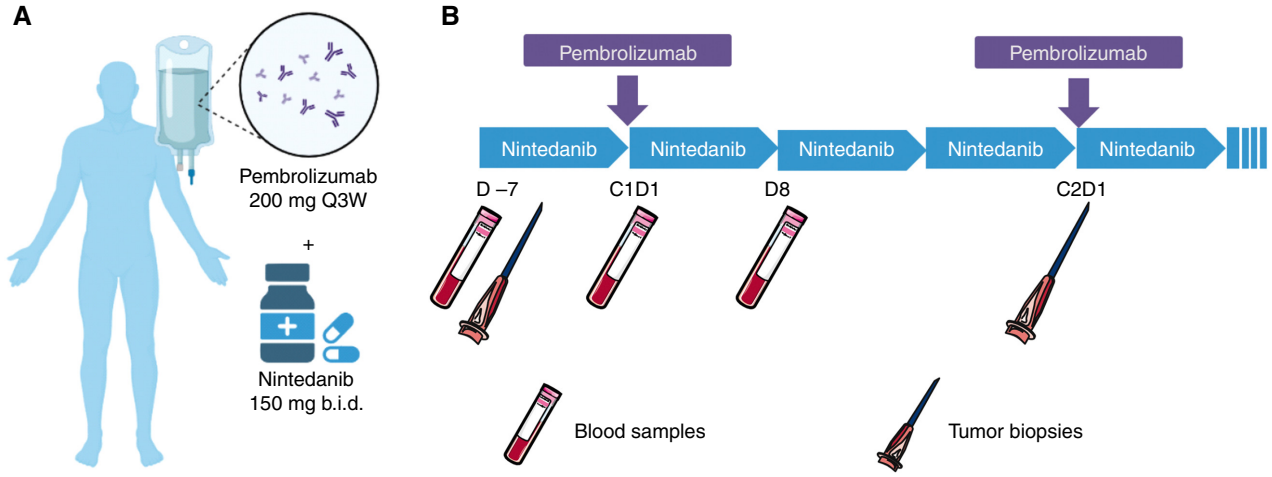

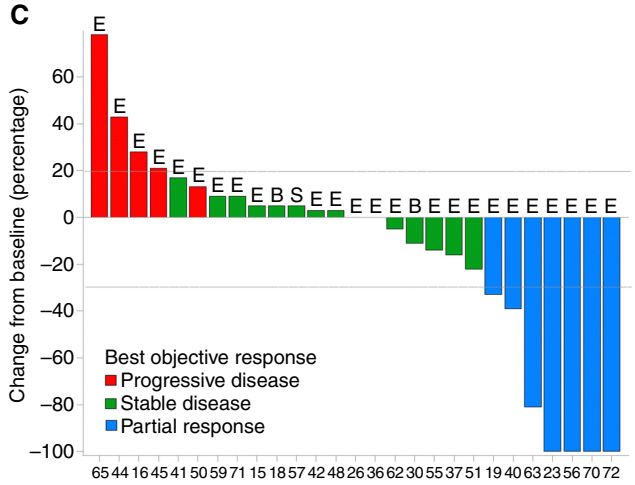

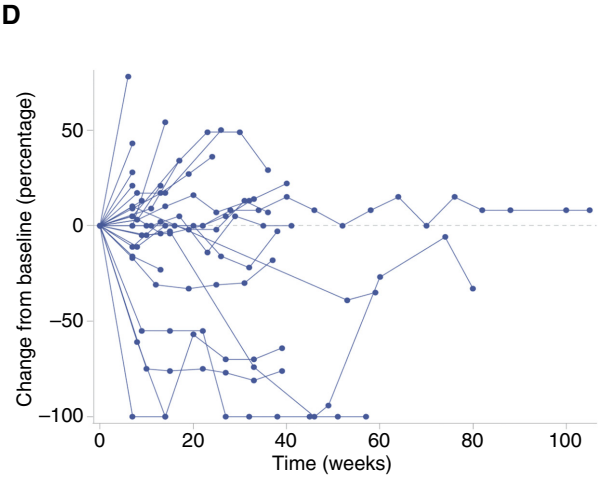

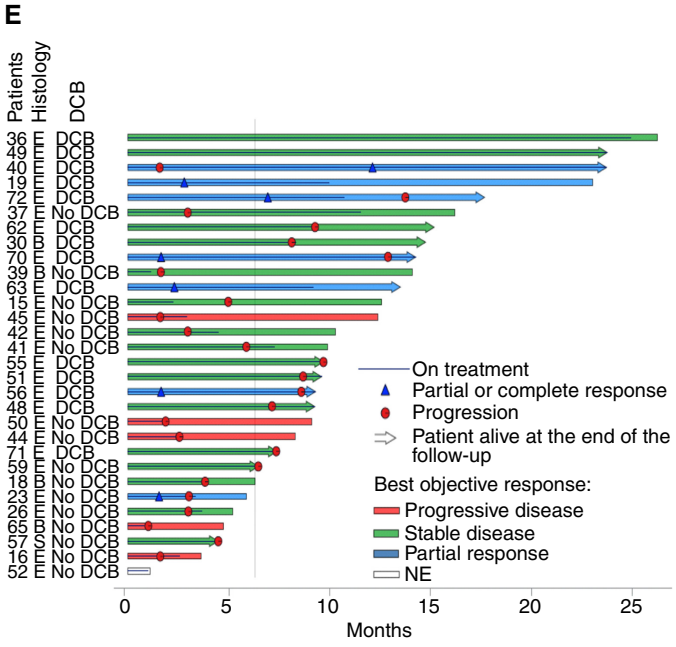

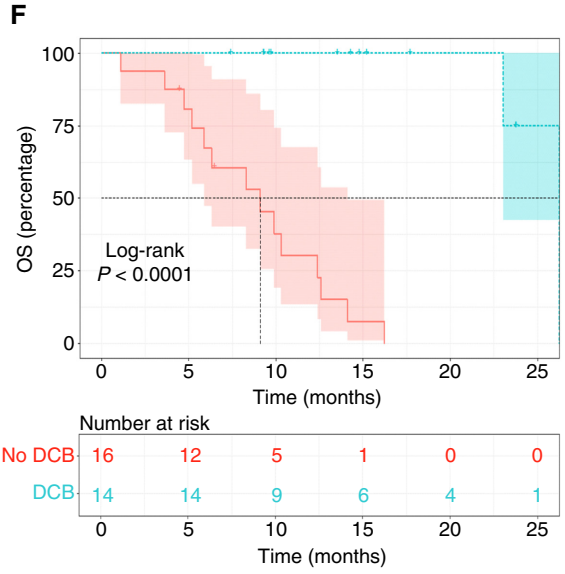

because of exclusion criteria, and 30 patients were treated in the trial. The baseline characteristics of the patients are described in Supplementary Table S1. The patients enrolled presented advanced tumors involving the pleura, with metastatic peritoneal carcinomatosis in 6 of 30 cases (20%), and were all refractory to or relapsing after first-line platinum-based doublet chemotherapy. The number of previous lines of treatment was 1, 2, and ≥3 for 23 of 30 (77%), 5 of 30 (17%), and 2 of 30 (6.7%) patients, respectively. Previous treatment with bevacizumab in combination with chemotherapy was reported for 12 of 30 (40%) patients.

Dose and/or scheduling modifications occurred in 12 of 29 (41%), and 4 of 29 (14%) patients because of adverse events (AE) associated with nintedanib and pembrolizumab, respectively. Treatment and dose modifications are summarized in Supplementary Table S2. Treatment-emergent AEs related to the study drugs per clinical investigator assessment are reported in Supplementary Table S3. The most frequent AEs (grades 1–3) related to the combination therapy were diarrhea, fatigue, nausea, and liver enzyme elevation. Twelve (40%) and 3 of 30 (10%) patients developed grade 3/4/5 treatment- and immune-related AEs, respectively [colitis with pneumonitis (n = 1) and myocarditis (n = 2), grade 3, 4, and 5, respectively]. Two patients developed arterial thrombosis [acute coronaropathy (n = 2) and mesenteric ischemia (n = 1)]. Patients died from cancer progression (n = 14/30, 46.7%); cardiopathy resulting in thrombosis and mesenteric ischemia, which may have been related to treatment (n = 1/30, 3.3%); and COVID-19 (n = 1/30, 3.3%). The patient who died of cardiopathy had a stage IV epithelioid pleural mesothelioma with peritoneal involvement, treated in first line with carboplatin pemetrexed. She was enrolled in the PEMBIB trial for her second line. During those initial weeks of treatment, she developed hyperthyroidism that was related to pembrolizumab and responsible for sinusal tachycardia. She did an echocardiography 1 week after starting pembrolizumab, which showed neither right nor left cardiac dysfunction; her left ventricle ejection fraction (LVEF) measured at that time was 60%. Circulating levels of brain natriuretic peptide (BNP) and troponin were also normal. At the C2D1 visit, she presented with sinusal tachycardia at 160 beats/minute, global cardiac insufficiency, and hyperthyroidism; BNP was increased (428 pmol/L), but blood troponin level was still normal. New echocardiography highlighted segmental myocardial dysfunction with altered LVEF (30%) and intracardiac thrombosis in the left ventricle. Corticosteroids were initiated with methylprednisolone 120 mg per day. Her clinical status rapidly deteriorated with hypotension and peripheral hypoperfusion. A CT-scan evaluation showed bilateral pulmonary embolism and arterial thromboses with intestinal and hepatic infarctions. An exploratory laparotomy was performed and confirmed a massive mesenteric infarction. She died 1 month after starting nintedanib (3 weeks after the first infusion of pembrolizumab) in multiple organ failure secondary to multiple vascular thrombosis and cardiomyopathy. Of note, lupus anticoagulant testing, and anticardiolipin and anti-beta2GP1 autoantibody tests were all negative. These AEs and her death were eventually attributed to both drugs.

Efficacy of Pembrolizumab + Nintedanib in Pleural Mesothelioma

The median follow-up of the cohort at database lock was 14.8 months [95% confidence interval (95% CI), 9.70–8.2)]. The median progression-free survival (PFS) was 6.2 months (95% CI, 3–8.7). At database lock, the median OS was 14.1 months (95% CI, 9.89–not reached). The median OS for patients with no durable clinical benefit (DCB) was 9.1 months (95% CI, 5.88–14.1) and 26.3 months for patients with DCB (95% CI, 23.03–not reached). One patient could not be evaluated for tumor response because of early death related to the above-mentioned grade 5 adverse event. Best objective responses (BOR) per RECIST version 1.1 (RECIST 1.1) criteria were partial response (PR; n = 7/29; 24.1%), stable disease (SD; n = 17/29; 58.6%), and progressive disease (n = 5/29; 17.2%; Fig. 1C). Disease control rates (defined as PR + SD) were 68.4% (95% CI, 43.4–87.4) and 46.6% at 3 and 6 months, respectively. At database lock, two patients (7%) ended treatment because they completed the 2-year treatment per protocol, but 23 of 30 (79%) had to stop because of cancer progression. Some patients presented durable tumor responses or durable SD (Fig. 1D). Therefore, for ancillary analysis, we decided to classify patients as having DCB (i.e., RECIST 1.1 PR or SD at 6 months after C1D1; called "DCB patients"), or having no clinical benefit (i.e., RECIST 1.1 PD before 6 months after C1D1; called "no DCB patients"; Fig. 1E). The baseline characteristics of the patients treated according to their DCB status is provided in Supplementary Table S4. We found that the 16 MM patients (53.3%) with no DCB per radiologic assessment had a very bad outcome compared with the 14 MM patients (46.7%) with radiologic DCB, as illustrated by their drastic differences in OS upon pembrolizumab + nintedanib therapy ($P < 0.0001$; Fig. 1F).

Predictive Biomarkers of Favorable Outcome

All patients enrolled in the PEMBIB trial consented to undergo blood draws and tumor biopsies at baseline and on treatment (Fig. 1B). Up to two cores of tumor biopsies were frozen and used for subsequent whole-exome sequencing (WES) and bulk gene expression analysis [RNA sequencing (RNA-seq)]. Up to two cores of tumor biopsies were formalin-fixed and paraffin-embedded for subsequent IHC stainings. Up to two cores of fresh tumor biopsies were immediately put into physiologic serum. Those biopsies were monitored for cytokine and soluble factor releases and then turned into cell suspensions for flow cytometry analysis (Fig. 2A). We prospectively analyzed the samples to characterize the biology of patients with no DCB and identify biomarkers associated with primary resistance to pembrolizumab + nintedanib.

First, we aimed to confirm the value of the two biomarkers that have been previously associated with the efficacy of checkpoint blockade immunotherapies in mesothelioma. Looking at tumor PD-L1 expression by IHC [PD-L1 SP263 assay, tumor proportion score (TPS) assessment], we could confirm that patients with DCB had higher PD-L1 expression on cancer cells than no DCB patients [median PD-L1 expression for patients with DCB was 2.5 (95% CI, 0–12.5) and 0 for patients with no DCB (95% CI, 0–0); Fig. 2B]. This difference was driven mostly by patients having objective

PRs on their RECIST 1.1 target lesions (Supplementary Fig. S1A). This finding was in accordance with the results recently generated in the above-mentioned randomized phase III trial of nivolumab + ipilimumab trial (tumor cell staining with the PharmDx 28-8 PD-L1 assay) in advanced MM naive of systemic therapies. Also, we performed bulk RNA-seq on baseline tumor biopsies and found a number of genes that were differentially expressed in DCB versus no DCB patients (Supplementary Fig. S1B). Gene set enrichment analysis (GSEA), with the "Hallmark" panels, identified 11 gene sets that were significantly differentially expressed in biopsies of patients with DCB (Fig. 2C; Supplementary Fig. S1C). Seven gene sets were upregulated and four were repressed in tumor biopsies of patients with DCB. Genes significantly upregulated in patients with DCB pertained to pathways related to oxidative phosphorylation (OXPHOS) metabolism, IFNα pathway, IFNγ pathway, and "allograft rejection" signature, suggesting an ongoing adaptive immune response in the tumor. Significantly suppressed pathways in tumors from patients with DCB (therefore relatively enriched in tumors primarily resistant to treatment) were genes from the EMT pathway, G_2–M checkpoint, and E2F and MYC targets. Those three E2F, MYC, and G2M pathways shared several downstream gene expressions (Supplementary Fig. S2).

The result on EMT gene upregulation in patients with no DCB is in accordance with the above-mentioned second biomarker recently reported to be associated with atezolizumab + bevacizumab resistance in refractory peritoneal MM. Beyond these reported predictive biomarkers, we found additional ones in the tumor and the blood by exploring fresh tumor biopsies and fresh whole blood.

First, flow cytometry analysis of fresh tumor biopsies at baseline found significantly more $CD45^+$, $CD3^+$, and $CD3^+CD8^+$ T cells in patients with DCB (Fig. 2D). Comparatively, IHC estimation of T-cell, B-cell, and macrophage infiltrations in screening tumor biopsies could not detect significant differences between patients with or without DCB (Supplementary Fig. S3A and Supplementary Table S5). Of note, the proportion of PD-1–positive $CD4^+$ or $CD8^+$ T cells was not significantly higher in patients with DCB, but there was a trend toward more $PD1^+$ $CD8^+$ T cells in patients subsequently developing PRs (Supplementary Fig. S3B).

Flow cytometry analysis of fresh whole blood identified increased levels of Th1 T cells in DCB patients, defined as $CD3^+CD4^+$ T cells expressing CXCR3, the receptor of CXCL9 and CXCL10 (Fig. 2E). More specifically, patients with DCB presented higher levels of circulating effector memory T cells expressing selectins (CLA) and integrins (a4b7, CD49a), which are typically prone to home into tissues (Fig. 2F).

Altogether, patients with DCB presented baseline features in their tumor and blood compatible with ongoing antitumor T-cell activity, which was expected to pave the way to a response to checkpoint blockade immunotherapy.

Pharmacodynamic Markers

We took advantage of the 1-week lead-in nintedanib monotherapy prior to pembrolizumab introduction to analyze the respective effects of the two drugs. Sequential blood sampling was performed at baseline and on-treatment in order to identify selective pharmacodynamic markers of nintedanib and pembrolizumab that occurred upon treatment in all patients and independently from the treatment efficacy. Plasma was obtained from blood draws collected at baseline (D −7), 1 week after the nintedanib monotherapy lead-in (C1D1), and 1 week after the addition of pembrolizumab (C1D8). First, we found that nintedanib monotherapy significantly decreased the levels of blood Angiopoitin-2, CCL21, and CCL23 in patients with both DCB and no DCB (Fig. 3A). CCL15 and CXCL10 were also decreasing in all patients upon nintedanib monotherapy, but this decrease was only significant for patients with DCB (Supplementary Fig. S4A). Of note, CCL8 significantly increased during this first week of nintedanib in patients with no DCB but tended to decrease in patients with DCB, suggesting potential opposite effects of antiangiogenics on CCL8 in these two patient categories (Supplementary Fig. S4B).

The addition of pembrolizumab at C1D1 had a rapid impact on blood levels of soluble PD-1 (sPD-1) and soluble PD-L1 (sPD-L1). Although circulating sPD1 levels were undetectable at baseline in all patients at C1D1, they reached median levels above 10 ng/mL in patients with both DCB and No DCB after a week (C1D8; Fig. 3B). Conversely, we found detectable circulating levels of sPD-L1 at baseline, which also significantly increased upon pembrolizumab therapy in all patients after 1 week (Fig. 3C). As opposed to the decrease of CCL21 found upon nintedanib lead-in monotherapy (Fig. 3A, middle), we found an increase in CCL19 in all patients after 1 week of combination with pembrolizumab, illustrating potential opposite impacts of the combination therapy on ligands of CCR7, a chemokine receptor expressed by memory T cells (Fig. 3D). Of note, CCL3, CCL8, CCL17, and CCL23 also increased, whereas CXCL2 levels decreased upon pembrolizumab addition, but this was significant only in patients with no DCB (Supplementary Fig. S4C).

Most surprising was the significant rise in CXCL9, CXCL10, CXCL11, and CXCL13 serum levels, which are potent Th1 and follicular T helper cell chemokines, respectively, just 1 week after initiation of pembrolizumab in patients with DCB but also with no DCB (Fig. 3E).

Active Recruitment of $CD8^+$ T Cells upon Treatment in the Tumors of Patients with No DCB

Patients prospectively underwent image-guided tumor biopsies at baseline and on treatment (C2D1 prior to second infusion of pembrolizumab). Fresh tumor biopsies were immediately put into physiologic serum. Each tumor secretome (i.e., tumor biopsy supernatant) was subsequently collected for titration of cytokines and soluble factors released by the tumor tissue. Also, fresh tumor biopsies were turned into cell suspensions upon mechanic dissociation for flow cytometry (see Fig. 2A and Methods).

In order to check if the elevated blood chemokines detected at C1D8 were also secreted by tumors and maintained 3 weeks after combination treatment initiation, we analyzed the supernatant of the fresh tumor biopsies

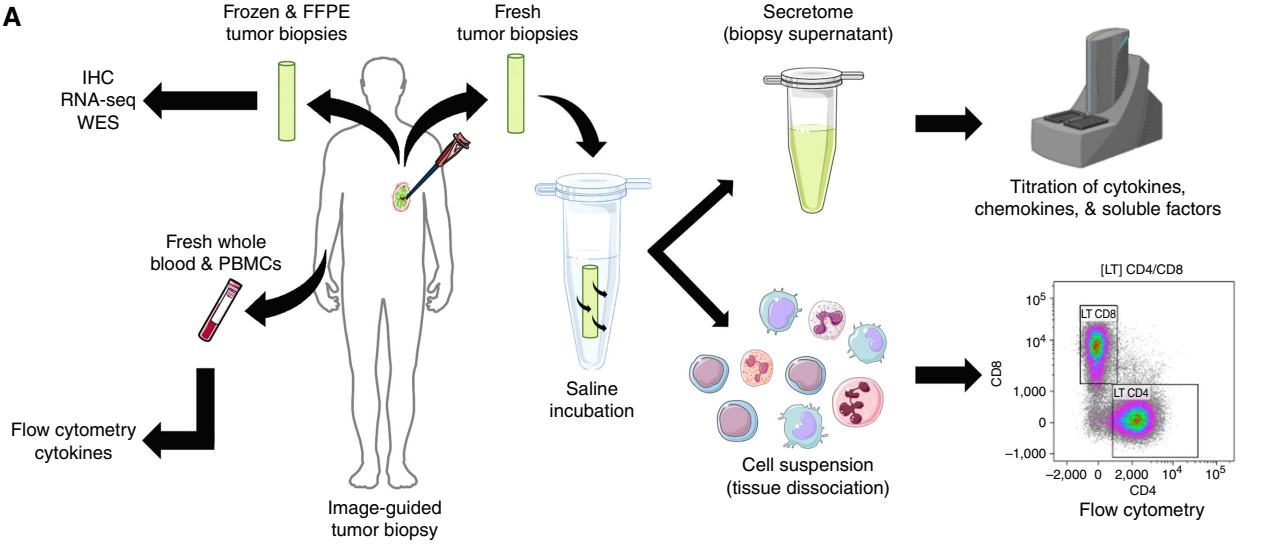

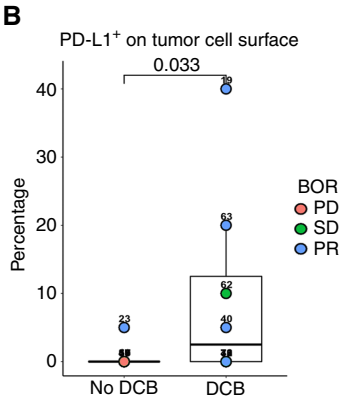

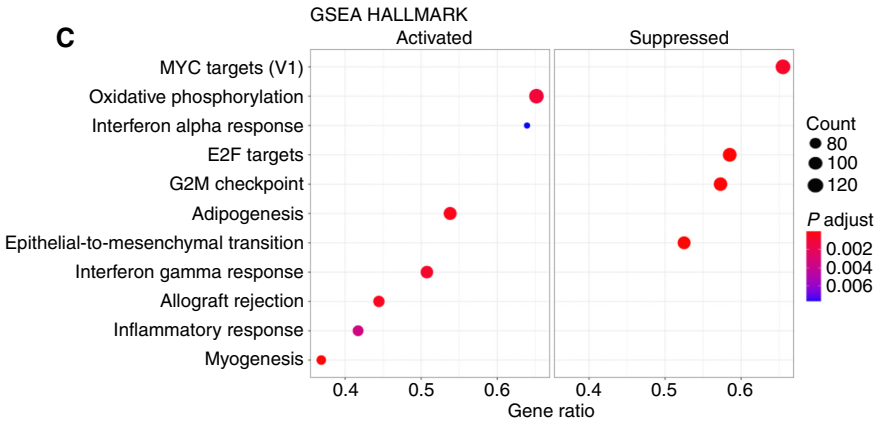

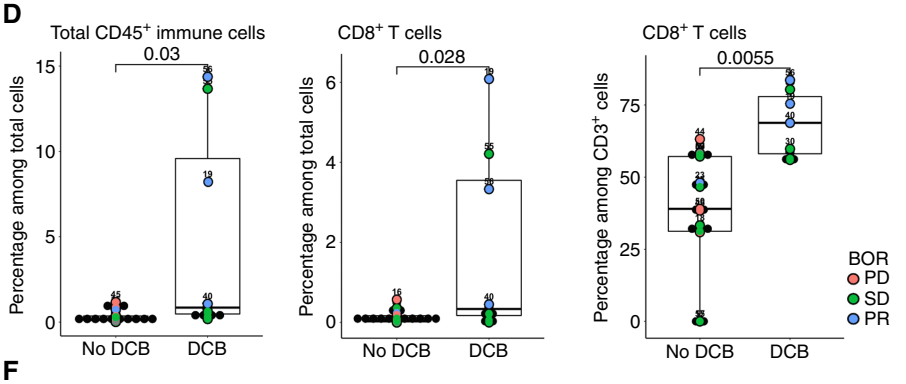

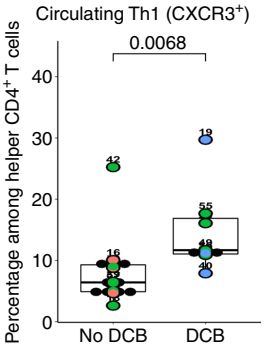

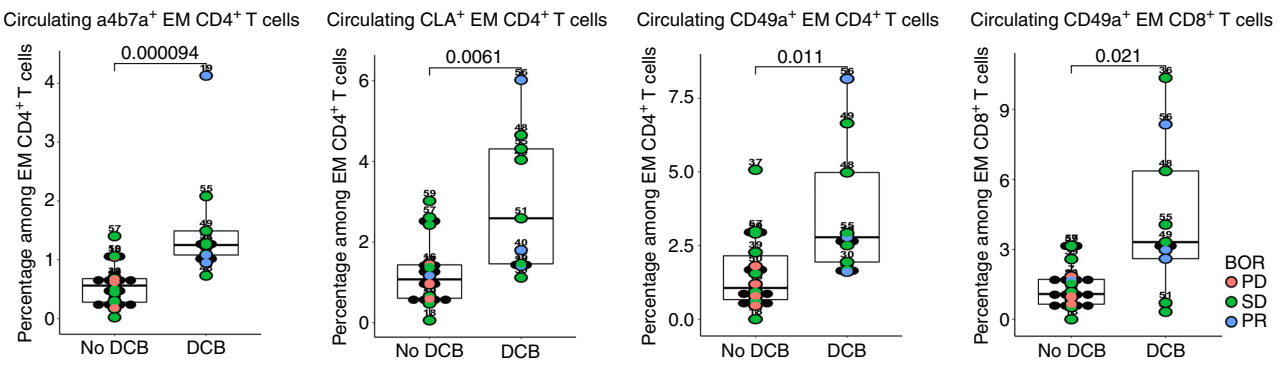

collected at C2D1. Within all the cytokines and chemokines titrated in the tumor biopsy supernatants, we found that CXCL9 was the most significant secreted cytokine by tumors between C2D1 and baseline (Fig. 4A). Indeed, we found a dramatic increase (~10×) of CXCL9 secretion by tumor biopsies between baseline and on treatment in patients with both DCB and no DCB but with higher values in the no DCB secretome (Fig. 4B).

Because CXCL9 is a potent T-cell chemoattractant, we wondered if those high levels of chemokine secretion would recruit T cells in the tumors. Analyzing the dynamics of T-cell infiltrates from the flow cytometry data collected from paired fresh tumor biopsies at baseline and at C2D1 (see the gating strategy in Supplementary Fig. S5), we found indeed a significant increase in CD45$^+$ (Fig. 4C, left), CD3$^+$ (Fig. 4D, left) and CD3$^+$ CD8$^+$ (Fig. 4E, left) T cells but predominantly in the tumors of patients with no DCB, who had very little T-cell infiltrates at baseline (Fig. 2D). The recruitment of those immune cells into tumors of patients with no DCB was also confirmed by absolute numbers of cells per biopsy by flow cytometry (Fig. 4C–E, right). The analysis of RNA-seq data from tumor biopsies also found an upregulation of CD8A, CD3e, and CD3z gene expression, which was significant only in patients with no DCB (Fig. 4F; Supplementary Fig. S6A). Interestingly, this T-cell fingerprint was associated with an upregulation of transcripts encoding for EOMES and T-bet transcription factors (Fig. 4G and H, respectively), IFNG (Supplementary Fig S6B), granulysin (Fig. 4I), and granzyme A and B (Fig. 4J), which all characterize cytotoxic effector T cells.

Unexpectedly, this active T-cell recruitment in tumors from patients with no DCB led to tumor CD8$^+$ T-cell infiltrates that were equivalent to patients with DCB within only 3 weeks of combination treatment, as we could not find any more differences in CD45$^+$, CD3$^+$, and CD3$^+$ CD8$^+$ T-cell infiltrates between patients with DCB and no DCB at C2D1 (Fig. 4K).

Of note, immune infiltration in tumor analyses with deconvolution of bulk RNA-seq data highlighted that the MCP counter score for T cells, CD8 T cells, natural killer cells, and cytotoxicity increased significantly between screening and C2D1 biopsies in no DCB patients (Supplementary Fig. S6C). Moreover, semiquantitative scoring of CD8 by IHC was not able to accurately recapitulate the flow cytometry and transcriptomic findings, although a trend toward increased densities of CD8$^+$ cells was found in tumors with objective radiologic responses upon combination treatment (Supplementary Figs. S3 and S6D).

Overall, we found that, upon pembrolizumab + nintedanib treatment, tumors from patients with no DCB secreted T cell–attracting chemokines and actively recruited CD8$^+$ T cells to a point that they were similar to tumors from patients with DCB only 3 weeks after C1D1.

Primary Resistance to Anti–PD-1 and Antiangiogenics Is Associated with an Increase in Intratumoral Activated Regulatory T Cells

In order to understand what was driving the resistance to anti–PD-1 + antiangiogenics, we further explored the blood and tumor samples prospectively collected from the patients with mesothelioma treated with pembrolizumab and nintedanib. First, we found that tumors from patients with no DCB presented with a significant increase in CD4$^+$ T-cell proportions upon treatment (Fig. 5A), resulting in more CD4$^+$ T cells at C2D1 in tumors from patients with no DCB (Fig. 5B). Within those intratumoral CD4$^+$ T cells, we found significantly higher proportions of CD25-expressing cells at C2D1 (Fig. 5C), although no difference in CD4$^+$CD25$^+$ T cells was found in biopsies at baseline (Supplementary Fig. S6E). The dynamics of CD4$^+$CD25$^+$ numbers was indeed increasing in tumor biopsies of patients with no DCB (Fig. 5D). Concomitantly, soluble CD25 in the secretome increased between screening and C2D1 in patients with no DCB as opposed to patients with DCB (Fig. 5E). Looking at the gene expression within those tumor biopsies, we also found higher TIGIT expression in patients with no DCB upon treatment (Fig. 5F), together with ICOS upregulation (Fig. 5G), CTLA4 (Fig. 5H), and FOXP3 (Fig. 5I).

Altogether, these observations suggest that upon pembrolizumab and nintedanib treatment, mesothelioma patients with no DCB present more intratumoral CD4$^+$ T cells with a phenotype compatible with activated regulatory T cells (Treg).

Primary Resistance to Anti–PD-1 and Antiangiogenics Is Associated with High VEGF, IL8, and IL6

In order to understand why, upon CXCL9 release, the recruitment of T cells into tumors of patients with no DCB was in favor of CD4$^+$ T cells with high CD25 expression and FOXP3 transcription, we looked for factors that have been described to sustain Treg expansion. First, we found that VEGFA was increasing in the secretome of the tumor biopsies from patients with no DCB (Fig. 6A). This resulted in significantly more VEGFA at C2D1 in the secretome of the tumor biopsies from patients with no DCB (Fig. 6B). Interestingly, this trend for VEGFA was not found in the blood (Supplementary Fig. S6F). However, a similar trend was found in the blood for VEGFD, which was higher at baseline in the plasma

Figure 2. Baseline tumor and systemic immune features of patients benefitting from pembrolizumab and nintedanib. **A,** Graphical representation of the techniques applied to fixed, frozen, and fresh blood and tumor samples prospectively collected and analyzed in the study. PBMC, peripheral blood mononuclear cell. **B,** Membrane PD-L1 expression by cancer cells by IHC (anti–PD-L1 staining clone SP263; TPS scoring) on baseline biopsies ($n = 20$) according to DCB status. **C,** GSEA (Hallmark panel) from RNA-seq data representing the genomic pathways significantly upregulated (activated) or downregulated (suppressed) in baseline tumor biopsies of patients with DCB (compared with those without DCB); $n = 13$ tumor samples, considering all genes differentially expressed ($P \leq 0.05$ adjusted with Benjamini–Hochberg method: Wald test; $n = 515$ genes). **D,** Evaluation of tumor immune infiltrate by flow cytometry after fresh tissue dissociation of baseline tumor biopsies between patients with DCB or no DCB ($n = 22$). **E,** Analyses of fresh blood samples by flow cytometry to phenotype circulating T lymphocytes before treatment initiation. Box plot representation of the percentage of circulating CXCR3$^+$ CCR4$^-$ CCR6$^-$ cells among helper memory CD4$^+$ T cells. **F,** Box plot representations of percentages of alpha-4 beta-7–positive (a4b7$^+$), cutaneous lymphocyte-associated antigen-positive (CLA$^+$) and CD49a-positive (CD49a$^+$) cells among circulating effector memory (EM) CD4$^+$ and CD8$^+$ T cells ($n = 25$). All tests were Wilcoxon rank-sum test (unpaired samples).

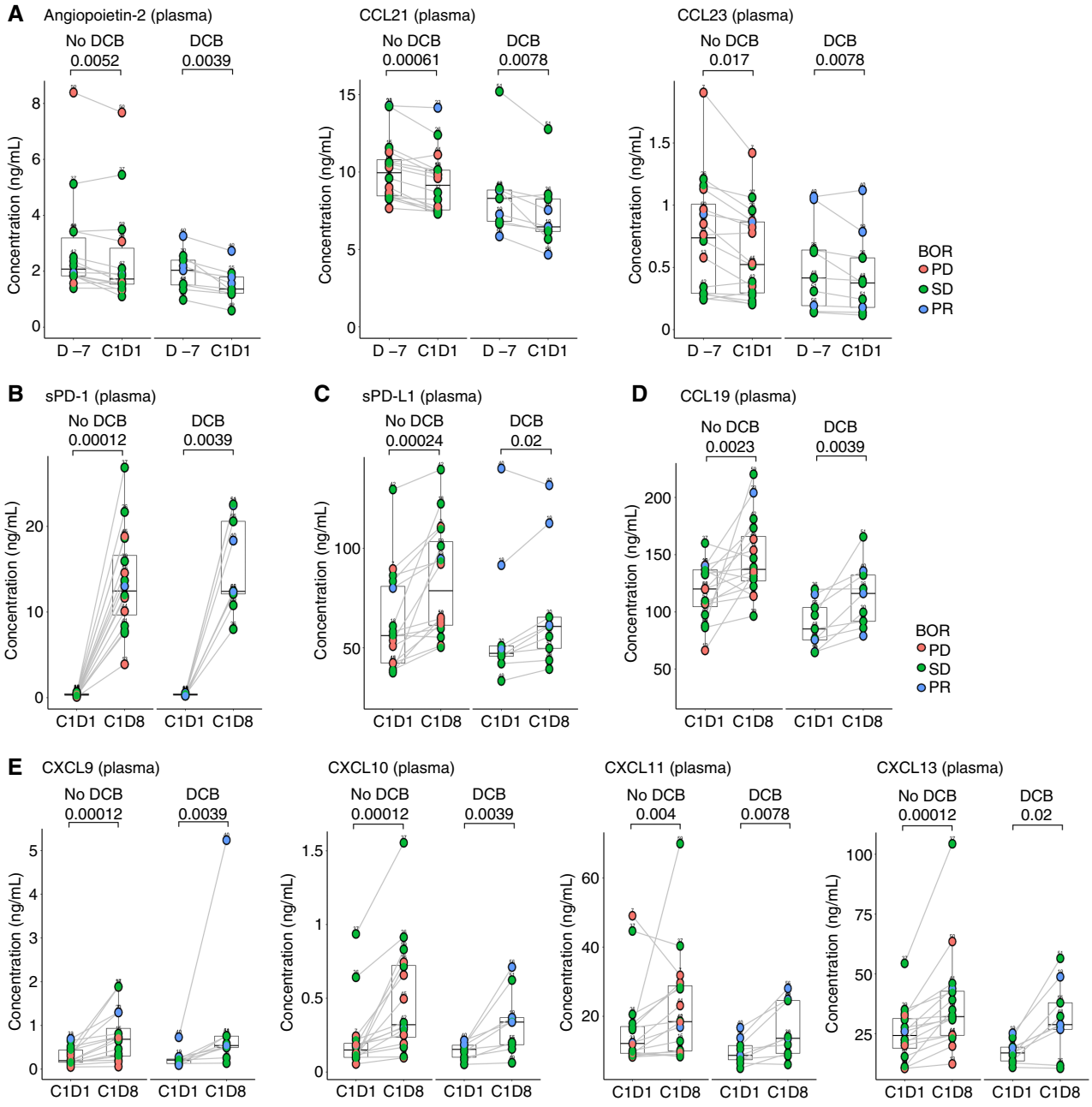

Figure 3. Pharmacodynamic markers of nintedanib monotherapy and upon addition of pembrolizumab. **A,** Paired plasmatic levels of angiopoietin-2, CCL21, and CCL23 before nintedanib lead-in monotherapy treatment (D –7) and after 7 days of daily treatment (C1D1). Paired plasmatic levels of sPD-1 (**B**), sPD-L1 (**C**), and CCL19 (**D**) after 1 week of nintedanib and before the addition of pembrolizumab (C1D1) and after 7 days of combination therapy (C1D8; $n = 25$). **E,** Evolution of paired plasma CXCL9, CXCL10, CXCL11, and CXCL13 concentrations between cycle 1 day 1 (C1D1) and after 1 week of nintedanib + pembrolizumab combination therapy (C1D8) for patients with and without DCB ($n = 25$). All statistical tests were paired Wilcoxon signed-rank test (paired samples).

of patients with no DCB (Fig. 6C) and tended to increase upon treatment in patients with no DCB, while decreasing in patients with DCB (Fig. 6D).

In order to understand what could support the secretion of VEGF molecules in patients with no DCB, we titrated the levels of CXCL8 (IL8) in the plasma of our patients and found significantly more circulating CXCL8 at baseline in patients with no DCB (Fig. 6E). Although CXCL8 levels remained stable and high upon treatment in the plasma of patients with no DCB (Fig. 6F), they tended to increase in their secretome (Fig. 6G). This resulted in significantly more CXCL8 in the secretome of patients with no DCB at C2D1 (Fig. 6H).

We also titrated IL6 because it has been frequently associated with CXCL8 expression and Treg development. We found

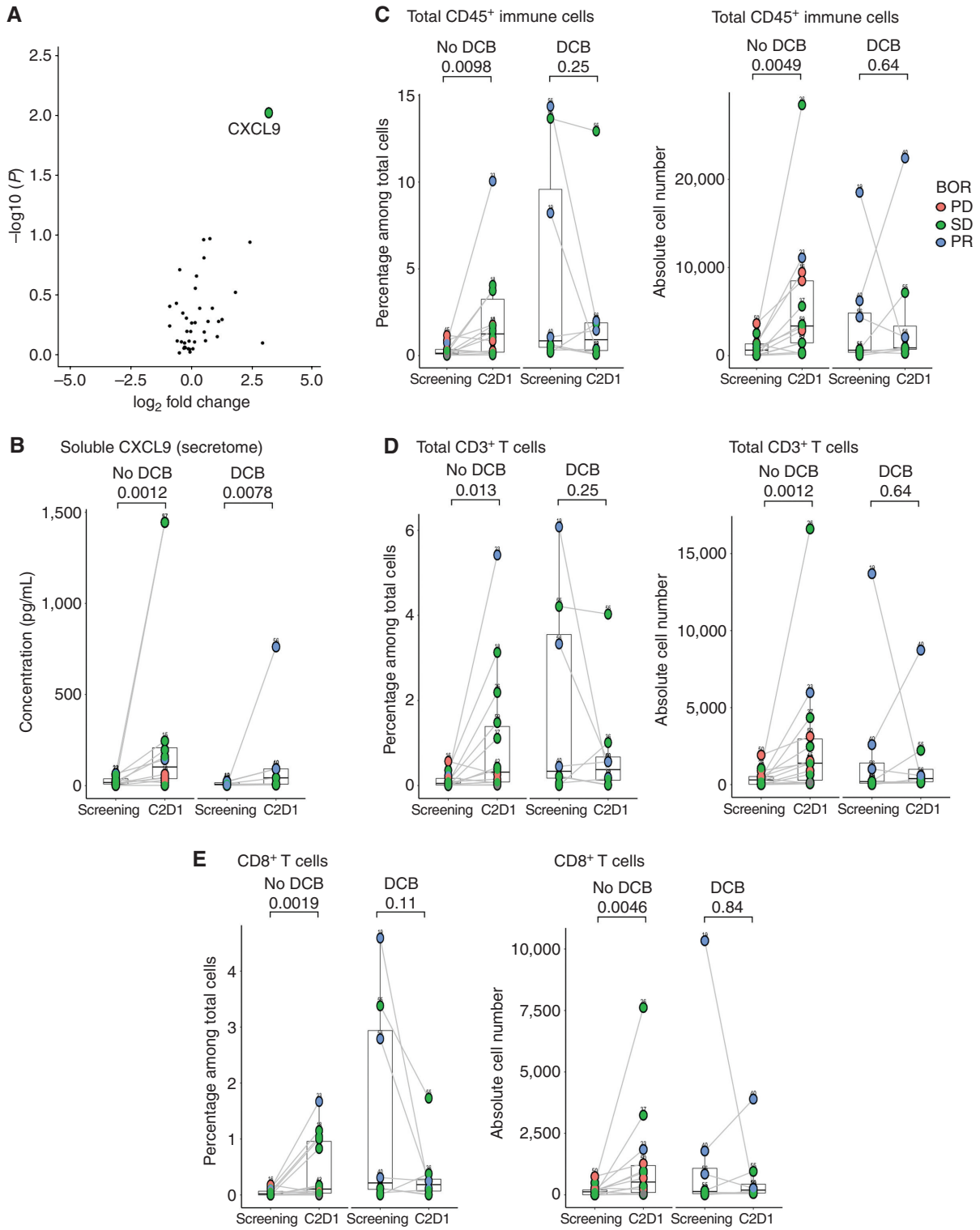

Figure 4. Patients with no DCB effectively recruit cytotoxic CD8+ T cells in their tumors upon pembrolizumab + nintedanib therapy. **A,** Volcano plot depicting the most secreted chemokines in the tumor secretome between baseline and C2D1 tumor biopsies (prior to second infusion of pembrolizumab). **B,** Paired comparisons of CXCL9 concentrations in the secretome of biopsies for patients with DCB or no DCB. **C,** Paired comparisons of CD45+ immune cells by proportions (percentage among total viable cells; left) and counts (absolute cell number; right) in tumor biopsies before (screening) and after 3 weeks of combination treatment (C2D1) in patients with DCB or no DCB. **D,** Paired comparisons of CD3+ T cells by proportions (percentage among total viable cells; left) and counts (absolute cell number; right) in tumor biopsies before (screening) and after 3 weeks of combination treatment (C2D1) in patients with DCB or no DCB. **E,** Paired comparisons of CD8+ T cells by proportions (percentage among total viable cells; left) and counts (absolute cell number; right) in tumor biopsies before (screening) and after 3 weeks of combination treatment (C2D1) in patients with DCB or no DCB. (*continued on next page*)

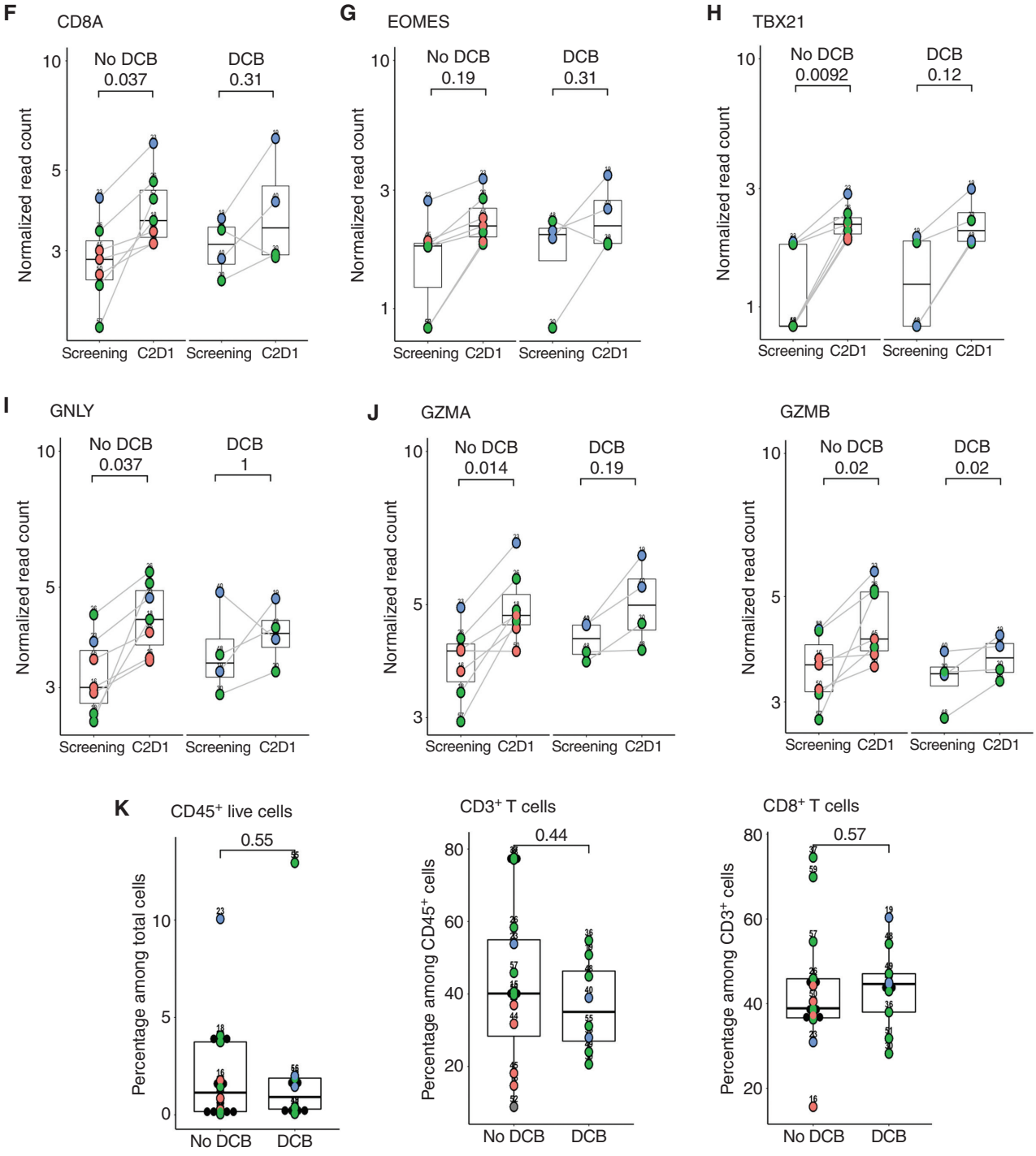

Figure 4. ***(Continued)*** **F–J**, CD8 alpha (CD8A), eomesodermin (EOMES), T-box transcription factor 21 (TBX21), granulysin (GNLY), granzyme A (GZMA; left), and granzyme B (GZMB; right) respective gene expression from RNA-seq data (normalized read counts) before (screening) and after 3 weeks of combination treatment (C2D1) in patients with DCB or no DCB. **K,** Absence of difference in the percentage of CD45+ immune cells among total viable cells (left), CD3+ T cells among CD45+ viable immune cells (middle), and CD8+ T cells among viable CD3+ T cells (right) in tumor biopsies of patients with no DCB compared with patients with DCB. All tests were paired Wilcoxon signed-rank test (paired comparisons) and Wilcoxon rank-sum test (unpaired comparisons).

high blood levels of IL6 at baseline (D −7; Fig. 6I). Those levels remained high upon the addition of nintedanib (C1D1; Fig. 6J) and pembrolizumab (C1D8; Fig. 6K). We found that one of the potential sources of IL6 in those patients was the tumor itself. Indeed, the concentrations of IL6 were high in the secretome of tumors from patients with no DCB, with a tendency to increase between baseline and C2D1 (Fig. 6L), resulting in significantly more IL6 at C2D1 (Fig. 6M).

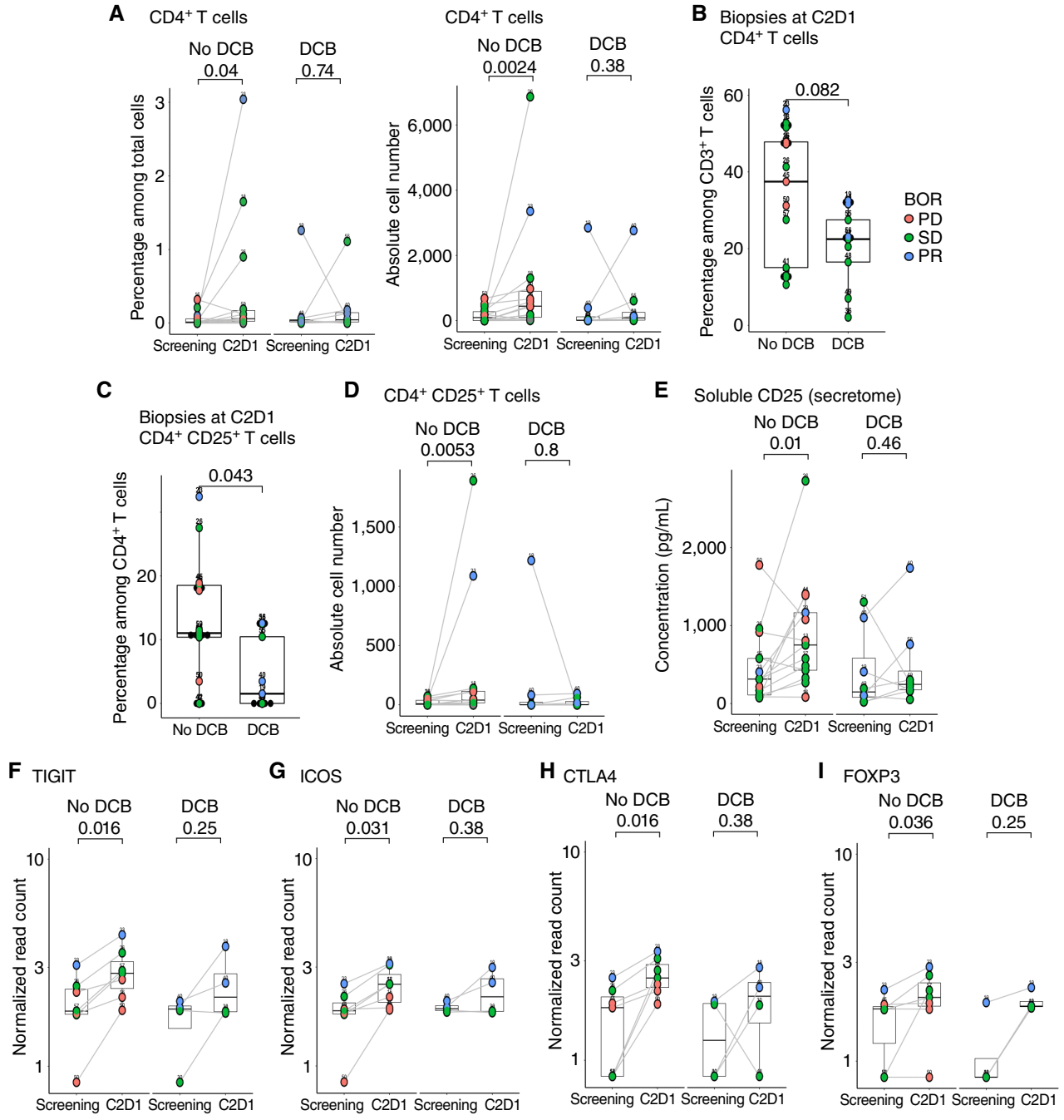

Figure 5. Patients with no DCB actively recruit CD4+ T cells with a regulatory phenotype in their tumors upon pembrolizumab + nintedanib therapy. **A,** Paired comparisons of CD4+ T cells by proportions (percentage among total viable cells; left) and counts (absolute cell number; right) in tumor biopsies before (screening) and after 3 weeks of combination treatment (C2D1) in patients with DCB or no DCB. **B** and **C,** Respective proportions of CD4+ cells among CD3+ T cells and CD4+CD25+ cells among CD4+ T cells in tumor biopsies of patients with no DCB compared with patients with DCB after 3 weeks of combination treatment (C2D1). **D,** Dynamics of CD4+CD25+ T-cell absolute cell counts in tumor biopsies of patients with no DCB compared with patients with DCB before (screening) and after 3 weeks of combination treatment (C2D1). **E,** Soluble CD25 in the secretome of tumor biopsies of patients with no DCB compared with patients with DCB after 3 weeks of combination treatment (C2D1). **F–I,** TIGIT, ICOS, CTLA4, and FOXP3 respective gene expression from RNA-seq data (normalized read counts) before (screening) and after 3 weeks of combination treatment (C2D1) in patients with DCB or no DCB. All tests were paired Wilcoxon signed-rank test (paired comparisons) and the Wilcoxon rank-sum test (unpaired comparisons).

Overall, those results illustrate that mesothelioma patients with no DCB have a systemic proinflammatory and proangiogenic profile at baseline with increased tumor secretion of IL6, CXCL8, and VEGF upon pembrolizumab and nintedanib therapy.

Genomic Somatic Copy-Number Alterations Correlate with Plasma IL6 Levels

To better understand the biological characteristics of mesotheliomas from patients refractory to anti–PD-1 and

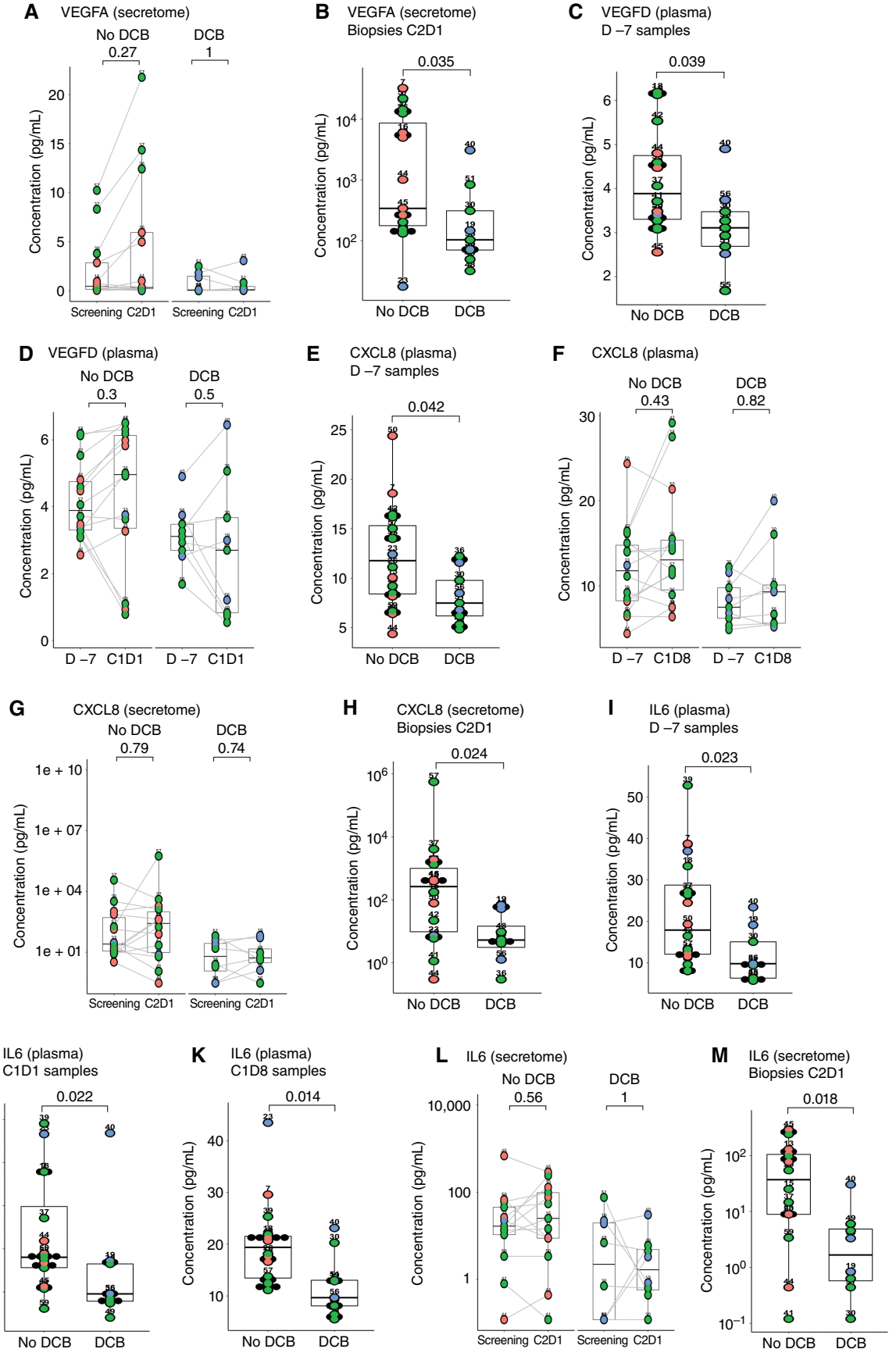

antiangiogenic therapy, we decided to analyze the oncogenetic profiles of the tumors collected during the trial.

As differential tumor gene expression analyses from RNA-seq at baseline identified that the E2F pathway was enriched in patients with no DCB, we looked for chromosome 9 alterations by fluorescent *in situ* hybridization (FISH), considering that 9p21 homozygous deletions are frequently described in mesothelioma and lead to CDKN2A deletion. We found indeed that patients with no DCB presented twice as many chromosome 9 alterations (homozygous deletions, monosomy, and heterozygous deletions) than patients with DCB (Fig. 7A and B).

Then, we performed WES from tumors collected during the trial in order to better understand the oncogenetic alterations found in our patients. Only 13 tumor biopsies were contributive (enough tumor material and sufficient proportions of cancer cells). We identified high numbers of somatic genomic alterations in patients with no DCB (Fig. 7C). Losses of tumor suppressor genes by point mutations and/or somatic copy-number alterations (SCNA) were identified in *BAP1* (67%), *EP300* (67%), *NF2* (61%), *SETD2* (61%), *CDKN2A* (56%), *CREBBP* (44%), *TP53* (39%), *MGA* (22%), and *DDX3X* (17%) genes. The median tumor mutational burden was 0.7 mutations per megabase (0.48–2.11).

We identified that patients with no DCB had a higher SCNA score than patients with DCB (Fig. 7D). Interestingly, we found a positive correlation between the number of SCNAs and IL6 plasma levels (Fig. 7E).

When integrating the different biomarkers described above into a single heat map, we found higher values of SCNAs with tumor and blood biomarkers associated with no DCB (Fig. 7F). Of note, the most consistent predictive biomarker for DCB was the proportion of $CD8^+$ cells among the total $CD3^+$ T cells, as assessed by flow cytometry on baseline fresh tumor biopsies (Figs. 2D and 7F).

DISCUSSION

Mesothelioma is one of the latest tumor indications in which the benefits of immunotherapy targeting the PD-1/PD-L1 pathway have been demonstrated. Here, we report that the combination of pembrolizumab 200 mg Q3W with nintedanib 150 mg b.i.d. provides significant antitumor activities and manageable toxicities in patients with advanced pleural mesothelioma naive to immunotherapy and refractory to the first line of platinum-based chemotherapy. Of note, pembrolizumab monotherapy in this patient population generated a best ORR (BORR) of 8% in the Keynote-158 study per RECIST 1.1 (16). Here, the addition of the antiangiogenic TKIs nintedanib and pembrolizumab compared favorably with this historical dataset, with a 3-fold higher BORR of 24% using the same radiologic criteria, although in a smaller patient population ($n = 30$ vs. $n = 118$). More recently, the combination of an intrapleural antimesothelin chimeric antigen receptor-T-cell therapy with pembrolizumab generated a BORR of 12.5% in the same patient population but with the modified RECIST criteria (21). Of note, those results need to be interpreted in their context: Outcomes obtained within clinical trials are always overestimating what could be achieved in a routine setting without close patient monitoring and without patient selection such as performance status and organ function. Also, the determination of 6 months as a landmark for our ancillary analysis of DCB is arbitrary and applied in our academic studies across cancer types. Larger studies are needed to establish whether another landmark time point would be more clinically relevant and biologically consistent to define DCB in mesothelioma. Because of our study's limited sample size, our clinical and biological results would need to be validated in larger trials.

Beyond clinical outcomes, the extensive biological explorations performed in this study shed light on the mechanisms associated with a primary resistance of pleural mesotheliomas to anti–PD-1 immunotherapy combined with antiangiogenic TKI. First, we confirm that a statistically significant higher expression of PD-L1 by IHC on cancer cells and that an epithelial rather than mesenchymal gene expression signature are found in mesothelioma tumors of patients having a better outcome under PD-1/PD-L1–targeted immunotherapies (17, 18). However, such biomarkers are poorly sensitive and specific at the individual level because of a broad overlap of values between patients with favorable and bad outcomes. The use of flow cytometry on fresh samples at baseline identified new and potentially more robust predictive biomarkers of outcome upon PD-1/PD-L1–targeted immunotherapy in mesothelioma, which are the proportion of $CD8^+$ T cells within the total tumor-infiltrating $CD3^+$ T cells, and high levels of effector memory T cells in the blood expressing selectins and integrins. The 7-day monotherapy lead-in allowed us to describe that the immediate pharmacodynamic effects of nintedanib were to diminish the circulating levels of

Figure 6. Primary resistance to pembrolizumab + nintedanib is associated with high VEGF, CXCL8, and IL6 concentrations in the blood and tumor of patients with mesothelioma. **A,** Paired comparisons of VEGFA concentrations in the secretome of tumor biopsies between baseline (screening) and after 3 weeks of combination treatment (C2D1) in patients with DCB and no DCB. **B,** Comparison of median values of VEGFA concentrations in the secretome of tumor biopsies after 3 weeks of combination treatment (C2D1) of patients with DCB and no DCB. **C,** Comparison of median values of VEGFD concentrations in the plasma at baseline (D –7) of patients with DCB and no DCB. **D,** Paired dynamics of VEGFD plasma concentrations during the first week of nintedanib monotherapy (D –7 vs. C1D1). **E,** Comparison of median CXCL8 concentration values in the plasma of DCB vs. no DCB patients at baseline (D –7). **F,** Paired comparisons of CXCL8 concentrations in the plasma of DCB vs. no DCB patients between baseline (D –7) and after 2 weeks of nintedanib and 1 week of pembrolizumab (C1D8). **G,** Paired comparisons of CXCL8 concentrations in the secretome of tumor biopsies of DCB vs. no DCB patients between baseline (screening) and after 3 weeks of combination treatment (C2D1). **H,** Comparison of median values of CXCL8 concentrations in the secretome of tumor biopsies after 3 weeks of combination treatment (C2D1) in patients with DCB and no DCB. **I–K,** Comparisons of median IL6 concentration values in the plasma of DCB vs. no DCB patients at baseline (D –7), after 7 days of nintedanib monotherapy (C1D1) and after 7 days of combination treatment (C1D8), respectively. **L,** Paired comparisons of IL6 concentrations in the secretome of tumor biopsies of DCB vs. no DCB patients between baseline (screening) and after 3 weeks of combination treatment (C2D1). **M,** Comparison of median values of IL6 concentrations in the secretome of tumor biopsies after 3 weeks of combination treatment (C2D1) in patients with DCB and no DCB. All tests were Wilcoxon rank-sum test (not paired samples) and paired Wilcoxon signed-rank test (paired samples).

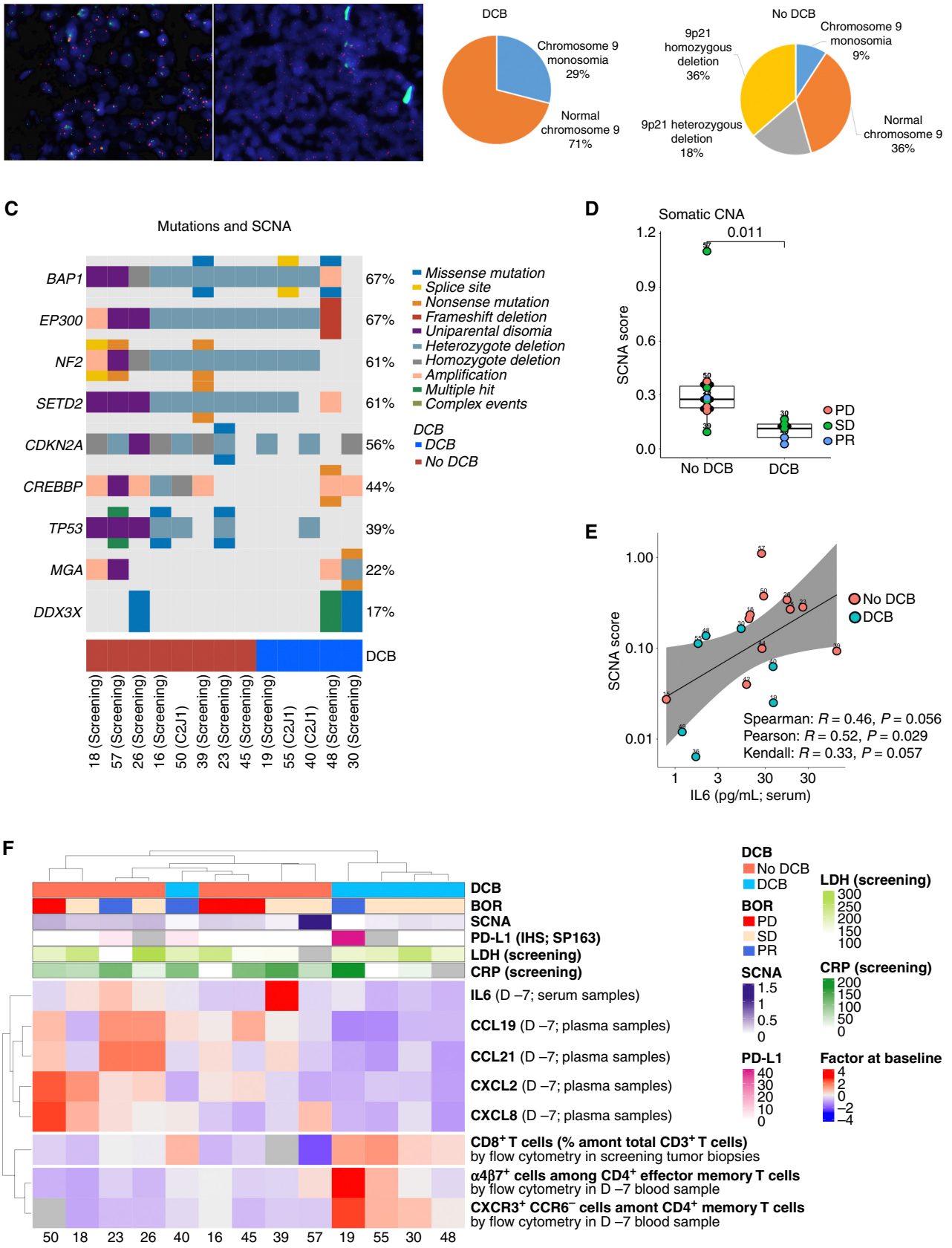

angiopoietin-2, CCL21, and CCL23, which are growth factors and proinflammatory chemokines known to be associated with mesothelioma pathogenesis (22–24). The addition of pembrolizumab increased dramatically in only 1 week the blood levels of CXCL9, and CXCL10, which are both potent T-cell attractants known to be pharmacodynamic effects of anti–PD-1 therapies (25). Here, we show that this effect also occurred in tumors, in which high levels of CXCL9 were detected in the secretome of all tumor biopsies 3 weeks after C1D1. Surprisingly, this CXCL9 burst was associated with a strong T-cell recruitment into tumors of patients with no DCB, notably $CD8^+$ T cells with a cytotoxic phenotype, which reached a proportion comparable with tumors of patients with DCB after only one cycle of treatment. The difference observed in tumor biopsies of the two subsets of patients was mostly regarding the $CD4^+$ T-cell composition of those immune infiltrates. Tumors from patients with no DCB presented a large proportion of $CD4^+$ T cells that presented features of activation compatible with an immunosuppressive Treg phenotype. One hypothesis that could explain why the phenotype of tumor-infiltrating T cells was skewed toward Tregs in tumors from patients with no DCB would be the preexisting proinflammatory and proangiogenic contexture of those tumors. Indeed, patients with no DCB presented high levels of VEGF, CXCL8 (IL8), and IL6 in both their blood and tumor secretome at baseline compared with patients with DCB, and those levels were even increased upon treatment. The VEGF pathways have recently been described as key pathologic features of human mesothelioma (12). A number of publications suggest that, across tumor types, VEGF molecules may play a role beyond angiogenesis and support immunosuppression within the TME via their direct effects on $CD8^+$ T cells (26), dendritic cells (27), and Tregs (28, 29). In mesothelioma, VEGF, CXCL8 and IL6 are well-known protumoral and autocrine factors (30–33). Interestingly, IL6 has been described to induce proliferation and VEGF expression in mesothelioma cancer cell lines (34). Although we could not find significant differences between subgroups of patients in terms of M1 or M2 macrophages according to CD68 and CD163 expression by IHC on tumor biopsies, it is possible that the phenotypes of tumor-infiltrative myeloid cells are playing an important role, as they are believed to be major sources of IL6, IL8, and VEGF in the TME. More surprising is our finding of a correlation between SCNAs and circulating levels of IL6. Some of the frequent somatic genomic alterations found in mesothelioma might indeed sustain the proinflammatory and proangiogenic phenotype of those tumors. For instance, TP53 mutations, frequently found in our patients with no DCB and typical genomic alterations of mesothelioma (35), have been shown to correlate with higher secretions of VEGF in NSCLC (36). Another frequent genomic alteration in mesothelioma that we found frequent in our patients with no DCB concerned chromosome 9, notably the 9p21 chromosomal region that contains the *CDKN2A* gene. CDKN2A is also a classic genomic alteration of mesothelioma (35). However, what is less known is the usual loss of type I IFN genes together with CDKN2A losses (37). Interestingly, those CDKN2A-associated type I IFN losses have been shown to present altered immune gene signatures in tumors (38). In myeloma cancer cell lines, which also frequently depend on IL6 autocrine signaling, it has been shown that the addition of IFNα in the culture media can downregulate the gene and protein expression of IL6 receptor subunits and therefore directly hamper the positive feedback loops of the pathway (39). Following the same reasoning, the loss of type I IFN expression in mesothelioma via 9p21 alterations could therefore support the autocrine IL6 growth signaling by the absence of downregulation of IL6 receptor subunits.

Overall, we found that patients with mesothelioma having primary resistance to PD-1–targeted immunotherapy and antiangiogenesis displayed high VEGF, CXCL8, and IL6 levels both in the blood and the tumor together with high genomic SCNAs. More mechanistic studies are needed to establish the link between such chromosomal instability and protumoral inflammation in mesothelioma.

The practical consequence of such biological characterization of patients with mesothelioma is an opportunity to better stratify their clinical care and offer biomarker-driven rather than simple histology-driven stratification of therapeutic strategies.

METHODS

Study Design

In this expansion cohort of the phase Ib clinical trial PEMBIB (NCT02856425), we evaluated the association of nintedanib (150 mg b.i.d.) in combination with i.v. flat doses of pembrolizumab 200 mg over 30 minutes Q3W. The posology of nintedanib was first determined in a dose-escalation cohort, which showed that nintedanib at 150 mg b.i.d. was better tolerated than 200 mg b.i.d. and subsequently selected for the expansion cohorts (40). Of note, patients received a 1-week lead-in course of nintedanib monotherapy prior to starting pembrolizumab. The protocol was first approved by the Agence Nationale de Sécurité du Médicament on June 24, 2016 (ref. #160371A-12). The protocol was also approved by the Ethical Committee (Comité de Protection des Personnes Ile de France 1) on July 12, 2016 (ref. #2016-mai-14236ND). The trial was first posted on ClinicalTrials.gov on August 4, 2016 (NCT02856425).

Figure 7. SCNAs are higher and correlate with IL6 levels in patients with primary resistance to pembrolizumab + nintedanib. **A,** Representative pictures of FISH analyses of 9p21 chromosomal region on FFPE tumor biopsy samples from a patient with DCB (patient #45, C2D1 biopsy, 9p21 heterozygous deletion; left) and no DCB (patient #16, screening biopsy, chromosome 9 monosomy; right). **B,** Proportions of chromosome 9 alterations in patients with DCB (left) and no DCB (right); 2/9 (29%) tumor biopsies presented chromosome 9 monosomy in DCB patients. Of patients with no DCB, 1/11 (9.1%) had chromosome 9 monosomy, 2/11 (18%) 9p21 heterozygous deletions, and 4/11 (36%) 9p21 homozygous deletions. **C,** Oncoplot representation of the principal genomic alterations found by WES analyses on tumor biopsies. Of note, uniparental disomia is a copy-neutral loss-of-heterozygosity. **D,** Comparison of the median score of SCNAs in tumor biopsies of patients with DCB and no DCB. Wilcoxon rank-sum test (unpaired samples). **E,** Linear correlation between SCNA score on tumor biopsies and IL6 plasma levels (Siemens assay). **F,** Unsupervised clustering heat map of the principal biomarkers identified illustrating the value of data generated on fresh samples to predict the outcomes of patients treated with anti–PD-1 and antiangiogenics in patients with mesothelioma. CRP, C-reactive protein; LDH, lactate dehydrogenase.

Patients

Eligible patients had advanced pleural mesothelioma that progressed after at least one line of standard therapy and was naive to immune-checkpoint blockade and nintedanib. Additional inclusion criteria included age ≥18 years, Eastern Cooperative Oncology Group performance status of 0 to 1, adequate organ function, measurable disease according to RECIST 1.1 criteria, and written informed consent. Key exclusion criteria were radiographic evidence of cavitary tumors, local invasion of major blood vessels and/or at risk for perforation, history of clinically significant hemoptysis within the past 3 months, history of clinically significant hemorrhagic or thromboembolic event in the past 6 months, history of significant cardiovascular diseases, prior treatment with nintedanib and anti–PD-(L)1 agents, concurrent steroid medication, and history of autoimmune and inflammatory disease. This study was conducted in compliance with the Declaration of Helsinki and the International Ethical Guidelines for Biomedical Research Involving Human Subjects.

Procedures

Screening procedures were performed up to 21 days (D −28) before D −7 (start of nintedanib). Patients continued treatment until disease progression, undue toxicity, withdrawal of consent, or for a maximum duration of 24 months. AEs were graded using the NCI Common Terminology Criteria for Adverse Events Version 4.03. Tumor responses were evaluated every 6 weeks based on RECIST 1.1 (41). Details about screening exams and other patient management rules are presented in the protocol of the trial provided in the supplementary information files.

Outcomes

The objectives of the trial were to determine the tolerability and safety of oral nintedanib 150 mg b.i.d. combined with i.v. pembrolizumab 200 mg Q3W and to evaluate the first efficacy signals with RECIST 1.1 BOR, PFS, and OS of this combination in a dedicated cohort of advanced MM. The aim of the ancillary studies was to identify predictive biomarkers of efficacy or resistance to this combination therapy.

Analyses of Tumor-Infiltrating Immune Cells from Biopsies by Flow Cytometry

Fine-needle biopsy samples from tumoral lesions were immediately placed into 1 mL of NaCl 0.9%. After a minimum of 30 minutes of incubation, the supernatant of fresh tumor biopsies in 0.9% NaCl was collected and frozen at −80°C, and biopsies were mechanically dissociated with the top of a 2-mL syringe plunger in a wet 70-μm filter placed at the top of a 50-mL centrifuge tube. Isolated cells were washed by centrifugation and resuspended in NaCl 0.9% for cell-surface staining protocol. Cells were stained with anti-CD3/BUV395 (clone UCHT1; ref. 563546, BD Biosciences), anti-CD4/BUV496 (clone SK3, ref. 564651, BD Biosciences), anti-CD45/BUV805 (clone HI30, ref. 612891, BD Biosciences), anti–PD-1/BV421 (clone MIH4, ref. 564323, BD Biosciences), anti-OX40/BV650 (clone ACT35, ref. 563658, BD Biosciences), anti-CD39/FITC (clone TU66, ref. 561444, BD Biosciences), anti–HLA-DR/PerCP5.5 (clone G46-6, ref. 551764, BD Biosciences), anti-CTLA4/PE (clone BNI3, ref. 555853, BD Biosciences), anti-41BB/PECF594 (clone 4B4-1, ref. 309826, BD Biosciences), anti-CD25/PECy7 (clone B1.49.9, ref. A52882, Beckmann Coulter), anti-TIGIT/APC (clone MBSA43, ref. 17-9500-41, BioLegend), anti–HLA-ABC/AF700 (clone W6/32, ref. 311438, BioLegend), anti-CD8/APC-H7 (clone SK1, ref. 560179, BD Biosciences), and Zombie Aqua Fixable Viability Kit (ref. 423101, BioLegend). CTLA4 was first stained at 37°C for 20 minutes before other surface antibodies were added and incubated at 4°C for 15 minutes. Then, cells were washed two times and acquired on an 18-color flow cytometer BD Fortessa X20 (BD Biosciences). Data were acquired in FCS 3.0 format and analyzed with Kaluza software version 2.1.

Immune Monitoring: Fresh Blood Immune Phenotype

Heparinized blood samples (30–40 mL) at D −7 (baseline), C1D1, and C5D1 were collected whenever possible for monitoring circulating immune populations by flow cytometry. Fresh whole blood phenotyping of T-cell migration, T-cell polarization, T-cell activation, Treg function, and myeloid cells was performed using five specific panels as previously described (42). Stained cells were acquired using a Gallios Cytometer (Beckman Coulter) and analyzed using Kaluza software (Beckman Coulter).

Cytokine, Chemokine, and Soluble Angiogenic Factor Measurements

Frozen plasma and frozen tumor biopsy supernatants were subsequently thawed, centrifuged for 15 minutes at 1,000 × *g*, and then titrated using the Bio-Plex ProTM Human Chemokine Panel (40-Plex, ref. 171AK99MR2, Bio-Rad), Angiogenesis Panel 1 (human; ref. K151P3S-1, Meso Scale Discovery), and Human PD-1 and PD-L1 antibody sets (ref. F214A-3 and F214C-3, Meso Scale Discovery) following the manufacturers' instructions. Each sample was run twice with the average value of the doublet taken as the result. Acquisitions were done on Bio-Plex 200TM System and Meso QuickPlex SQ120 readers. Raw data from Meso Scale Discovery's kit were analyzed with Meso Scale Discovery's Discovery Workbench 4.0.

Serum IL6 quantifications were subsequently confirmed with Siemens Atellica IM1600 and Atellica IM Interleukin-6 kit (Siemens Healthineers) and validated by the Gustave Roussy–accredited biochemistry diagnostic laboratory. Quantification method validation was performed according to ISO15189 recommendation. The quantification range covers from 2.7 (limit of quantification) to 5,500 pg/mL. Any quantification batches included three levels of internal quality control analysis. IL6 titrations obtained by Siemens were well correlated to the ones obtained on Bio-Rad.

IHC

IHC chromogenic staining was performed on FFPE tumor biopsies. PD-L1 (staining was performed using the SP263 PD-L1 assay) single chromogenic staining was performed using the Ventana Benchmark Ultra platform. CD20 staining and CD3 (Purple)/CD8 (DAB) chromogenic dual staining were performed using the Ventana Discovery Ultra platform. Tumor areas were selected by a senior pathologist blinded to the outcome of the patients.

FISH

FISH tests were performed on FFPE tumor tissues using ZytoLight SPEC CDKN2A/CEN 9 Dual Color Probe according to the manufacturer's instructions (ZytoVision). The SPEC CDKN2A/CEN 9 Dual Color Probe is a mixture of an orange fluorochrome directly labeled CEN 9 probe specific for the classic satellite III region of chromosome 9 (D9Z3) at 9q12 and a green fluorochrome directly labeled SPEC CDKN2A probe specific for the CDKN2A gene at 9p21.3. Slides were deparaffinized and then preincubated with the pretreatment buffer (citric solution) at 98°C for 15 minutes followed by protease treatment for 15 minutes at 37°C. After washes and dehydration with ethanol, slides were denatured at 75°C for 10 minutes and then hybridized with the probe overnight at 37°C. After several washes the following day, counterstain was added to the slides [4′6-diamidino-2-phenylindole (DAPI)]. Fifty cells were counted on each tumor sample categorizing signals as follows, counting the number of green signal and red signals in each cell: loss of one green signal and normal red signals (loss of one copy of CDKN2A); loss of two green signals and normal red signals

(loss of two copies of CDKN2A); loss of one green signal and one red signal (loss of a whole chromosome 9 or short arm); and normal red and green signals (normal cell).

Whole-Transcriptome RNA-seq

Integrity (RNA Integrity Score ≥7.0) of RNA extracted from frozen tumoral biopsies was checked on the Agilent 2100 Bioanalyzer (Agilent), and quantity was determined using NanoDrop (Thermo Fisher Scientific). The SureSelect Automated Strand-Specific RNA Library Preparation Kit was used according to the manufacturer's instructions with the Bravo Platform. Briefly, 50 to 200 ng of total RNA sample was used for poly-A mRNA selection using oligo (dT) beads and subjected to thermal mRNA fragmentation. The fragmented mRNA samples were used for cDNA synthesis and were further converted into double-stranded DNA using the reagents supplied in the kit, and the resulting double-stranded DNA was used for library preparation. The final libraries were barcoded, purified, pooled together in equal concentrations, and processed for paired-end 2 × 100 sequencing on a NovaSeq 6000 sequencer (Illumina) at Gustave Roussy.

Bulk Tumor RNA-seq Analyses

The quality control and analysis pipeline was based on Love and colleagues, powered by SnakeMake (43, 44). Quality controls were performed on raw FastQ files with FastQC v0.11.9. Read trimming for low 3′ terminal base quality and removal of adapter sequences was performed using fastp v0.20.1. Sample contamination was assessed with FastqScreen v0.14.0. Quality reports were gathered with MultiQC v1.9 (45). Abundance estimation was performed with Salmon v1.4.0, using 100 bootstraps and the GenCode v34 annotations, corresponding to the GRCh38 genome build (46). Aggregation was performed with the tximport package, and differential gene analysis was performed with DESeq2, with a formula design taking care of the sample effect when sample pairs (Screening/C2J1) were taken into consideration (47). Deconvolution of immune cell fractions from bulk RNA-seq data was done with immunedeconv package (48). GSEA and overrepresentation analysis were performed with the clusterProfiler package v4.0.2, against the Molecular Signatures Database (MSigDB) collections, Disease Ontology, and the Kyoto Encyclopedia of Genes and Genomes (KEGG), CellMarker, and MeSH databases (49). For quality control, the variance stabilizing transformation (vst) normalization from DESeq2 was applied on raw counts. Of note, RNA-seq data from baseline biopsies without tumor cells were not integrated into the analyses. Also, the data from the baseline pleural biopsy for patient #23, who had a peritoneal progression before 6 months, were considered in the "DCB" group because of a primary and persistent complete response of pleural lesions.

Somatic and Germline WES

Fifty to 200 ng of genomic DNA was extracted from frozen tumor biopsies with the Covaris E220 system (LGC Genomics/Kbioscience). DNA fragments were end-repaired, extended with an "A" base on the 3′ end, ligated with paired-end adapters with the Bravo Platform (Agilent), and amplified (10 cycles). Exome-containing adapter-ligated libraries were hybridized for 40 hours with biotinylated oligo RNA baits using SureSelect Clinical Research 2 (Agilent) and enriched with streptavidin-conjugated magnetic beads. The final libraries were indexed, pooled, and sequenced using the onboard cluster method as paired-end sequencing (2 × 100 bp reads) on an Illumina NovaSeq 6000 sequencer at Gustave Roussy.

WES Analyses

Identification of mutations and individual SCNAs was done with the following methods: Reads were mapped using the BWA-MEM (v0.7.12) software (50) to the GRCh37 human reference genome, and then we used the standard GATK best practice pipeline (51) to process the samples and call somatic genetic variants. PCR duplicates were removed, and the base quality score was recalibrated using MarkDuplicates and BaseRecalibrator tools, which are a part of the GATK package (52). Somatic single-nucleotide variants and insertions and deletions (INDEL) were called and filtered using the GATK tools Mutect2, FilterMutectCalls, and FilterByOrientationBias and annotated with oncotator (53). Quality controls of FASTQ and mapping were done with FASTQC, samtools (v1.9), GATK Hsmetrics, and multiqc (45, 54). The processing steps were combined in a pipeline built with snakemake (44). Somatic mutations with PASS flag from GATK Mutect2 were additionally filtered to have at least one supporting read from each strand and three reads in total. We then used the Mutation Annotation Format annotator to find oncogenic mutations from the OncoKB database and visualized them as an oncoplot with the maftools R package (55). Tumor mutational burden of the samples was calculated in accordance with the guidelines proposed by the Friends of Cancer Research TMB Harmonization Project (56).

Identification of copy-number alterations was performed using EaCoN v0.3.6 (https://github.com/gustaveroussy/EaCoN) on R v3.6.2. Per-patient paired samples were analyzed using tumoral samples as a test, and genomic DNA from peripheral blood mononuclear cells was used as a reference for each pair. GATK-recalibrated BAM files were transformed to the mpileup format using Rsamtools v2.8.0, ignoring replicates and secondary alignments (doi: 10.18129/B9.bioc.Rsamtools). The depth of each nt for test and reference was computed using mpileup and then binned to windows of 50 nt in median (depending on the capture BED information). Bins with a total depth <20 were discarded. Using a pregenerated track of GC% content in bins, those with a value <20% or >80% were identified as outliers. Still for each bin, median depths were converted to log2(Test/Ref) (L2R), and L2R for GC% outliers was imputed using kNN. L2R was then normalized for GC% using a lowess regression. To generate the BAF data, any nonreference sequences in the mpileups were identified and their depth was quantified (57). SNP variants supported by less than 3 reads and/or for which the total depth was below 20 were discarded. All SNP variants in the test sample with a reference frequency below 33% were discarded. The bivariate (L2R and BAF) data were then segmented, evaluated for their allele-specific absolute copy number, as well as ploidy and tumor cellularity using ASCAT v2.5.2.

SCNA genomic instability score was established as follows: for each sample, the absolute copy-number (ACN) profile generated by ASCAT through EaCoN was used. For each chromosome taken independently, the basal ACN level was identified as the one with the longest total width. Then, for each chromosome, ACN levels were converted into the absolute difference to this basal level [aDCN = (i.e., if the basis was 3 copies, a 1 copy segment value will be 2; 2 copies ≥ 1; 3 copies ≥ 0; 4 copies ≥ 1; etc.)]. The final SCNA score was computed as the width-ponderated sum of each of these converted CN-to-basis values, divided by the total covered genome length.

Statistical Analysis and Illustrations

Clinical statistical analysis has been done using SAS statistical software version 9.4. Calculations and statistical tests for ancillary analyses were performed using R v3.4. Wilcoxon–Mann–Whitney test was used to assess differences between two patient groups. Data representation and analyses were performed with software R v3.3.3 using tidyverse, dplyr, ggplot2, ggpubr, complexheatmap, survival, and atable packages. Figure aesthetics were improved with Affinity Designer (v1.9.2.1035). Statistical tests applied to ancillary analysis were exploratory. *P* values were adjusted for multiple comparisons only for the differential gene expression analysis in transcriptomic data from screening tumor biopsies between patients with

or without DCB. All other *P* values in the article were not adjusted for multiple comparisons

Data Availability

Data from the PEMBIB clinical trial are available from the corresponding authors upon reasonable request. The data are not publicly available due to information that could compromise the privacy of the research participants.

Authors' Disclosures

S. Mouraud reports grants and nonfinancial support from Boehringer Ingelheim and nonfinancial support from Merck Sharp & Dohme during the conduct of the study. C. Baldini reports other support from Bicycle Therapeutics, MSD, Amgen, Iteos, Janssen, and AstraZeneca and grants from Bristol Myers Squibb outside the submitted work. A. Varga reports other support from AstraZeneca outside the submitted work. A. Rabeau reports personal fees from Bristol Myers Squibb and MSD outside the submitted work. S. Champiat reports personal fees (honoraria) from Amgen, Astellas, AstraZeneca, Bristol Myers Squibb, Eisai, Genmab, Janssen, Merck, Merck Serono, Novartis, and Roche, grants from AbbVie, Amgen, Boehringer Ingelheim, Cytovation, Eisai, Imcheck Therapeutics, Molecular Partners, Merck, Ose Pharma, Pierre Fabre, Sanofi-Aventis, Sotio, and Transgene, personal fees (advisory board/consulting) from Alderaan Biotechnology, Amgen, AstraZeneca, Avacta, Celanese, Domain Therapeutics, Ellipses Pharma, Genmab, Immunicom, Nanobiotix, Oncovita, Pierre Fabre, Seagen, Tatum Bioscience, Tollys, and UltraHuman8, and personal fees (travel and congress) from Amgen, AstraZeneca, Bristol Myers Squibb, Merck, Ose Pharma, Roche, and Sotio outside the submitted work; is part of the Drug Development Department (DITEP); is a principal/sub-investigator of clinical trials for AbbVie, Adaptimmune, Adlai Nortye USA, Aduro Biotech, Agios Pharmaceuticals, Amgen, Astex Pharmaceuticals, AstraZeneca, Aveo, Basilea Pharmaceutica International, Bayer HealthCare, Bbb Technologies, BeiGene, BicycleTx, Blueprint Medicines, Boehringer Ingelheim, Boston Pharmaceuticals, Bristol Myers Squibb, Ca, Casi Pharmaceuticals, Celgene, Cellcentric, Chugai Pharmaceutical, Cullinan-Apollo, Curevac, Daiichi Sankyo, Debiopharm, Eisai, Eisai Limited, Eli Lilly, Exelixis, Faron Pharmaceuticals, Forma Therapeutics, Gamamabs, Genentech, GSK, H3 Biomedicine, F. Hoffmann-La Roche, Imcheck Therapeutics, Incyte, Innate Pharma, Institut De Recherche Pierre Fabre, Iris Servier, Iteos Belgium, Janssen-Cilag, Janssen Research Foundation, Janssen R&D, Kura Oncology, Kyowa Kirin Pharm. Dev, Lilly France, Loxo Oncology, MedImmune, Menarini Ricerche, Merck Sharp & Dohme Chibret, Merrimack Pharmaceuticals, Merus, Molecular Partners, Nanobiotix, Nektar Therapeutics, Novartis Pharma, Octimet Oncology, Oncoethix, Oncopeptides, Orion Pharma, Genomics, Ose Pharma, Pfizer, PharmaMar, Pierre Fabre Médicament, Relay Therapeutics, Roche, Sanofi-Aventis, Seattle Genetics, Sotio, Syros Pharmaceuticals, Taiho Pharma, Tesaro, Transgene, Turning Point Therapeutics, and Xencor; research grants from AstraZeneca, Bristol Myers Squibb, Boehringer Ingelheim, GSK, INCA, Janssen-Cilag, Merck, Pfizer, Roche, and Sanofi; and nonfinancial support (drug supplied) from AstraZeneca, Bristol Myers Squibb, Boehringer Ingelheim, GSK, MedImmune, Merck, NH TherAGuiX, Pfizer, and Roche. D. Bredel reports grants from Gustave Roussy during the conduct of the study. S. Susini reports grants and other support from Boehringer Ingelheim and Merck Sharp & Dohme during the conduct of the study. L. Tselikas reports grants from the Bristol Myers Squibb Foundation and Terumo Corporation, and personal fees from AstraZeneca, GE Healthcare, Boston Scientific, Servier, and Quantum Surgical outside the submitted work. J.-E. Fahrner reports other support from Transgene outside the submitted work. B. Besse reports grants from 4D Pharma, AbbVie, Amgen, Aptitude Health, AstraZeneca, BeiGene, Blueprint Medicines, Boehringer Ingelheim, Celgene, Cergentis, Chugai Pharmaceutical, Cristal Therapeutics, Daiichi Sankyo, Eli Lilly, Eisai, Genzyme Corporation, GSK, Inivata, Ipsen, Janssen, Onxeo, OSE Immunotherapeutics, Pfizer, Roche/Genentech, Sanofi, Takeda, Tolero Pharmaceuticals, and Turning Point Therapeutics during the conduct of the study. J. Adam reports personal fees from MSD and Amgen, and grants from Bayer outside the submitted work. L. Zitvogel reports grants from the Seerave Foundation, 9 Meters, Pileje, and Daiichi Sankyo, and personal fees from EverImmune and Hookipa during the conduct of the study. N. Chaput reports personal fees from AstraZeneca France, grants from Bristol Myers Squibb and Sanofi, and other support from Cytune Pharma outside the submitted work. C. Massard reports consulting/advisory fees from Amgen, Astellas, AstraZeneca, Bayer, BeiGene, Bristol Myers Squibb, Celgene, Debiopharm, Genentech, Ipsen, Janssen, Lilly, MedImmune, MSD, Novartis, Pfizer, Roche, Sanofi, and Orion, and is a principal/sub-investigator of clinical trials for AbbVie, Aduro, Agios, Amgen, Argen-x, Astex, AstraZeneca, Aveo Pharmaceuticals, Bayer, BeiGene, Blueprint, Bristol Myers Squibb, Boehringer Ingelheim, Celgene, Chugai, Clovis, Daiichi Sankyo, Debiopharm, Eisai, Eos, Exelixis, Forma, Gamamabs, Genentech, Gortec, GSK, H3 Biomedicine, Incyte, Innate Pharma, Janssen, Kura Oncology, Kyowa, Lilly, Loxo, Lysarc, Lytix Biopharma, MedImmune, Menarini, Merus, MSD, Nanobiotix, Nektar Therapeutics, Novartis, Octimet, Oncoethix, Oncopeptides, Orion, Pfizer, PharmaMar, Pierre Fabre, Roche, Sanofi, Servier, Sierra Oncology, Taiho, Takeda, Tesaro, and Xencor. J.-C. Soria reports personal fees from Amgen and other support from Amgen, Gritstone Bio, and Relay Therapeutics outside the submitted work. C. Gomez-Roca reports grants, personal fees, and other support from Roche/Genentech, grants and personal fees from Bristol Myers Squibb, other support from Pierre Fabre and MSD, personal fees and other support from Macomics, personal fees from Ellipses and Foundation Medicine, and grants from Amgen outside the submitted work. G. Zalcman reports grants from the Roche Foundation, personal fees, nonfinancial support, and other support from Bristol Myers Squibb, personal fees and other support from AstraZeneca, Sanofi, and Pfizer, and other support from AbbVie outside the submitted work. D. Planchard reports grants from Gustave Roussy during the conduct of the study; personal fees from AstraZeneca, Daiichi Sankyo, Novartis, Pfizer, Roche, Janssen, AbbVie, Bristol Myers Squibb, and MSD outside the submitted work; clinical trial research as principal or coinvestigator (institutional financial interests) for AstraZeneca, Bristol Myers Squibb, Boehringer Ingelheim, Eli Lilly, Merck, Novartis, Pfizer, Roche, MedImmune, Sanofi-Aventis, Taiho Pharma, Novocure, Daiichi Sankyo, Janssen, and AbbVie; and travel, accommodations, and expenses from AstraZeneca, Roche, Novartis, and Pfizer. A. Marabelle reports other support from Merck Sharp & Dohme and grants and other support from Boehringer Ingelheim during the conduct of the study; personal fees, nonfinancial support, and other support from Merck Sharp & Dohme, personal fees from Boehringer Ingelheim, and grants from Fondation MSD Avenir outside the submitted work; and a patent for biomarkers of response to immunotherapy in mesothelioma pending. No disclosures were reported by the other authors.

Authors' Contributions

F.-X. Danlos: Data curation, software, formal analysis, validation, investigation, visualization, methodology, writing–original draft. **M. Texier:** Data curation, formal analysis, methodology. **B. Job:** Data curation, software, formal analysis, visualization. **S. Mouraud:** Data curation, software, formal analysis, validation, visualization, methodology. **L. Cassard:** Data curation,

formal analysis. **C. Baldini:** Investigation. **A. Varga:** Investigation. **A.A. Yurchenko:** Data curation, software, formal analysis, visualization, methodology. **A. Rabeau:** Investigation. **S. Champiat:** Investigation. **D. Letourneur:** Data curation, formal analysis, visualization. **D. Bredel:** Data curation, formal analysis, visualization. **S. Susini:** Data curation, formal analysis, visualization. **Y. Blum:** Formal analysis, supervision. **A. Parpaleix:** Data curation, investigation. **C. Parlavecchio:** Data curation, supervision, investigation, writing–original draft, data acquisition. **L. Tselikas:** Software, formal analysis, supervision, investigation, methodology, writing–original draft. **J.E. Fahrner:** Software, formal analysis, methodology. **A.-G. Goubet:** Software, formal analysis, methodology. **M. Rouanne:** Data curation, formal analysis, investigation. **S. Rafie:** Data curation, investigation. **A. Abbassi:** Data curation, investigation. **I. Kasraoui:** Formal analysis, investigation. **M. Breckler:** Data curation, formal analysis, investigation. **S. Farhane:** Data curation, investigation. **S. Ammari:** Investigation. **S. Laghouati:** Resources, data curation, formal analysis, validation, investigation, protocol writing. **A. Gazzah:** Formal analysis, investigation. **L. Lacroix:** Data curation, formal analysis, investigation. **B. Besse:** Data curation, software, formal analysis, validation, investigation, visualization, methodology. **N. Droin:** Data curation, software, formal analysis, validation, investigation, visualization, methodology. **M. Deloger:** Data curation, software, formal analysis, validation, visualization, methodology. **S. Cotteret:** Data curation, software, formal analysis, validation, visualization, methodology, writing–original draft. **J. Adam:** Data curation, software, formal analysis, validation, visualization, methodology, writing–original draft. **L. Zitvogel:** Data curation, software, formal analysis, validation, investigation, visualization, methodology, writing–original draft. **S.I. Nikolaev:** Data curation, software, formal analysis, supervision, validation, investigation, visualization, methodology, writing–original draft. **N. Chaput:** Data curation, software, formal analysis, supervision, investigation, visualization, methodology. **C. Massard:** Conceptualization, resources, data curation, software, formal analysis, supervision, funding acquisition, validation, investigation, visualization, methodology. **J.-C. Soria:** Conceptualization, resources, supervision, funding acquisition, investigation. **C. Gomez-Roca:** Conceptualization, resources, supervision, funding acquisition, investigation, writing–original draft. **G. Zalcman:** Resources, data curation, validation, investigation, writing–review and editing. **D. Planchard:** Resources, data curation, investigation, writing–original draft. **A. Marabelle:** Conceptualization, resources, data curation, formal analysis, supervision, funding acquisition, validation, investigation, visualization, methodology, writing–original draft, project administration, writing–review and editing, writing revised manuscript and answer to reviewers.

Acknowledgments

Pembrolizumab was kindly supplied by Merck Sharp & Dohme. Boehringer Ingelheim kindly provided nintedanib and funded most of the operational costs of the trial and its ancillary analysis. Gustave Roussy was the sponsor of the study and provided in-kind support for the execution of the trial. Gustave Roussy partly funded the medical and staff time of F.-X. Danlos, M. Texier, B. Job, S. Mouraud, L. Cassard, C. Baldini, A. Varga, A.A. Yurchenko, S. Champiat, A. Parpaleix, C. Parlavecchio, L. Tselikas, S. Rafie, A. Abbassi, I. Kasraoui, M. Breckler, S. Farhane, S. Ammari, S. Laghouati, A. Gazzah, L. Lacroix, B. Besse, N. Droin, M. Deloger, S. Cotteret, J. Adam, L. Zitvogel, S.I. Nikolaev, N. Chaput, C. Massard, J.-C. Soria, D. Planchard, and A. Marabelle. J.-E. Fahrner was funded by Transgene, and A.-G. Goubet was funded by Fondation pour la Recherche Médicale. A grant obtained from Fondation MSD Avenir partly funded the salaries of S. Mouraud, D. Bredel, and M. Rouanne. The University of Paris-Saclay also partly funded the salaries of F.-X. Danlos, L. Zitvogel, N. Chaput, C. Massard, J.-C. Soria, and A. Marabelle. L. Zitvogel was supported by the Germano-French ANR Ileobiome: 19-CE15-0029-01 and H2020 ONCOBIOME N°825410, RHU Torino Lumière ANR-16-RHUS-0008; Seerave Foundation; and SIRIC Stratified Oncology Cell DNA Repair and Tumor Immune Elimination (SOCRATE).

The publication costs of this article were defrayed in part by the payment of publication fees. Therefore, and solely to indicate this fact, this article is hereby marked "advertisement" in accordance with 18 USC section 1734.

Note

Supplementary data for this article are available at Cancer Discovery Online (http://cancerdiscovery.aacrjournals.org/).

Received August 8, 2022; revised November 25, 2022; accepted January 18, 2023; published first January 20, 2023.

REFERENCES

1. Galateau-Salle F, Churg A, Roggli V, Travis WD, World Health Organization Committee for Tumors of the Pleura. The 2015 World Health Organization classification of tumors of the pleura: advances since the 2004 classification. J Thorac Oncol 2016;11:142–54.
2. Xu A, Wu LJ, Santella RM, Hei TK. Role of oxyradicals in mutagenicity and DNA damage induced by crocidolite asbestos in mammalian cells. Cancer Res 1999;59:5922–6.
3. Dostert C, Pétrilli V, Van Bruggen R, Steele C, Mossman BT, Tschopp J. Innate immune activation through Nalp3 inflammasome sensing of asbestos and silica. Science 2008;320:674–7.
4. Vogelzang NJ, Rusthoven JJ, Symanowski J, Denham C, Kaukel E, Ruffie P, et al. Phase III study of pemetrexed in combination with cisplatin versus cisplatin alone in patients with malignant pleural mesothelioma. J Clin Oncol 2003;21:2636–44.
5. Musk AW, Olsen N, Alfonso H, Reid A, Mina R, Franklin P, et al. Predicting survival in malignant mesothelioma. Eur Respir J 2011;38:1420–4.
6. Grothey A, Galanis E. Targeting angiogenesis: progress with anti-VEGF treatment with large molecules. Nat Rev Clin Oncol 2009;6:507–18.
7. Ribas A, Wolchok JD. Cancer immunotherapy using checkpoint blockade. Science 2018;359:1350–5.
8. Finn RS, Qin S, Ikeda M, Galle PR, Ducreux M, Kim TY, et al. Atezolizumab plus bevacizumab in unresectable hepatocellular carcinoma. N Engl J Med 2020;382:1894–905.
9. Rini BI, Plimack ER, Stus V, Gafanov R, Hawkins R, Nosov D, et al. Pembrolizumab plus axitinib versus sunitinib for advanced renal-cell carcinoma. N Engl J Med 2019;380:1116–27.
10. Socinski MA, Jotte RM, Cappuzzo F, Orlandi F, Stroyakovskiy D, Nogami N, et al. Atezolizumab for first-line treatment of metastatic nonsquamous NSCLC. N Engl J Med 2018;378:2288–301.
11. Wallin JJ, Bendell JC, Funke R, Sznol M, Korski K, Jones S, et al. Atezolizumab in combination with bevacizumab enhances antigen-specific T-cell migration in metastatic renal cell carcinoma. Nat Commun 2016;7:12624.
12. Alcala N, Mangiante L, Le-Stang N, Gustafson CE, Boyault S, Damiola F, et al. Redefining malignant pleural mesothelioma types as a continuum uncovers immune-vascular interactions. EBioMedicine 2019;48:191–202.
13. Zalcman G, Mazieres J, Margery J, Greillier L, Audigier-Valette C, Moro-Sibilot D, et al. Bevacizumab for newly diagnosed pleural mesothelioma in the mesothelioma avastin cisplatin pemetrexed study (MAPS): a randomised, controlled, open-label, phase 3 trial. Lancet 2016;387:1405–14.
14. Grosso F, Steele N, Novello S, Nowak AK, Popat S, Greillier L, et al. Nintedanib plus pemetrexed/cisplatin in patients with malignant

pleural mesothelioma: phase II results from the randomized, placebo-controlled LUME-Meso trial. J Clin Oncol 2017;35:3591–600.
15. Scagliotti GV, Gaafar R, Nowak AK, Nakano T, van Meerbeeck J, Popat S, et al. Nintedanib in combination with pemetrexed and cisplatin for chemotherapy-naive patients with advanced malignant pleural mesothelioma (LUME-Meso): a double-blind, randomised, placebo-controlled phase 3 trial. Lancet Respir Med 2019;7:569–80.
16. Yap TA, Nakagawa K, Fujimoto N, Kuribayashi K, Guren TK, Calabrò L, et al. Efficacy and safety of pembrolizumab in patients with advanced mesothelioma in the open-label, single-arm, phase 2 KEYNOTE-158 study. Lancet Respir Med 2021;9:613–21.
17. Raghav K, Liu S, Overman MJ, Willett AF, Knafl M, Fu SC, et al. Efficacy, safety, and biomarker analysis of combined PD-L1 (atezolizumab) and VEGF (bevacizumab) blockade in advanced malignant peritoneal mesothelioma. Cancer Discov 2021;11:2738–47.
18. Baas P, Scherpereel A, Nowak AK, Fujimoto N, Peters S, Tsao AS, et al. First-line nivolumab plus ipilimumab in unresectable malignant pleural mesothelioma (CheckMate 743): a multicentre, randomised, open-label, phase 3 trial. Lancet 2021;397:375–86.
19. Nowak AK, Lesterhuis WJ, Kok PS, Brown C, Hughes BG, Karikios DJ, et al. Durvalumab with first-line chemotherapy in previously untreated malignant pleural mesothelioma (DREAM): a multicentre, single-arm, phase 2 trial with a safety run-in. Lancet Oncol 2020;21:1213–23.
20. Forde PM, Anagnostou V, Sun Z, Dahlberg SE, Kindler HL, Niknafs N, et al. Durvalumab with platinum-pemetrexed for unresectable pleural mesothelioma: survival, genomic and immunologic analyses from the phase 2 PrE0505 trial. Nat Med 2021;27:1910–20.
21. Adusumilli PS, Zauderer MG, Rivière I, Solomon SB, Rusch VW, O'Cearbhaill RE, et al. A phase I trial of regional mesothelin-targeted CAR T-cell therapy in patients with malignant pleural disease, in combination with the anti–PD-1 agent pembrolizumab. Cancer Discov 2021;11:2748–63.
22. Magkouta S, Kollintza A, Moschos C, Spella M, Skianis I, Pappas A, et al. Role of angiopoietins in mesothelioma progression. Cytokine 2019;118:99–106.
23. Jiang Q, Ghafoor A, Mian I, Rathkey D, Thomas A, Alewine C, et al. Enhanced efficacy of mesothelin-targeted immunotoxin LMB-100 and anti–PD-1 antibody in patients with mesothelioma and mouse tumor models. Sci Transl Med 2020;12:eaaz7252.
24. Ostroff RM, Mehan MR, Stewart A, Ayers D, Brody EN, Williams SA, et al. Early detection of malignant pleural mesothelioma in asbestos-exposed individuals with a noninvasive proteomics-based surveillance tool. PLoS One 2012;7:e46091.
25. Letourneur D, Danlos FX, Marabelle A. Chemokine biology on immune checkpoint-targeted therapies. Eur J Cancer 2020;137:260–71.
26. Voron T, Colussi O, Marcheteau E, Pernot S, Nizard M, Pointet AL, et al. VEGF-A modulates expression of inhibitory checkpoints on CD8+ T cells in tumors. J Exp Med 2015;212:139–48.
27. Gabrilovich DI, Chen HL, Girgis KR, Cunningham HT, Meny GM, Nadaf S, et al. Production of vascular endothelial growth factor by human tumors inhibits the functional maturation of dendritic cells. Nat Med 1996;2:1096–103.
28. Li B, Lalani AS, Harding TC, Luan B, Koprivnikar K, Tu GH, et al. Vascular endothelial growth factor blockade reduces intratumoral regulatory T cells and enhances the efficacy of a GM-CSF-secreting cancer immunotherapy. Clin Cancer Res 2006;12:6808–16.
29. Terme M, Pernot S, Marcheteau E, Sandoval F, Benhamouda N, Colussi O, et al. VEGFA-VEGFR pathway blockade inhibits tumor-induced regulatory T-cell proliferation in colorectal cancer. Cancer Res 2013;73:539–49.
30. Rahim SNA, Ho GY, Coward JIG. The role of interleukin-6 in malignant mesothelioma. Transl Lung Cancer Res 2015;4:55–66.
31. Nowak AK, Brosseau S, Cook A, Zalcman G. Antiangiogeneic strategies in mesothelioma. Front Oncol 2020;10:126.
32. Galffy G, Mohammed KA, Dowling PA, Nasreen N, Ward MJ, Antony VB. Interleukin 8: an autocrine growth factor for malignant mesothelioma. Cancer Res 1999;59:367–71.
33. Donnenberg AD, Luketich JD, Donnenberg VS. Secretome of pleural effusions associated with non-small cell lung cancer (NSCLC) and malignant mesothelioma: therapeutic implications. Oncotarget 2019;10:6456–65.
34. Adachi Y, Aoki C, Yoshio-Hoshino N, Takayama K, Curiel DT, Nishimoto N. Interleukin-6 induces both cell growth and VEGF production in malignant mesotheliomas. Int J Cancer 2006;119:1303–11.
35. Yap TA, Aerts JG, Popat S, Fennell DA. Novel insights into mesothelioma biology and implications for therapy. Nat Rev Cancer 2017;17:475–88.
36. Schwaederlé M, Lazar V, Validire P, Hansson J, Lacroix L, Soria JC, et al. VEGF-A expression correlates with TP53 mutations in non-small cell lung cancer: implications for antiangiogenesis therapy. Cancer Res 2015;75:1187–90.
37. Grard M, Chatelain C, Delaunay T, Pons-Tostivint E, Bennouna J, Fonteneau JF. Homozygous co-deletion of type I interferons and CDKN2A genes in thoracic cancers: potential consequences for therapy. Front Oncol 2021;11:695770.
38. Peng Y, Chen Y, Song M, Zhang X, Li P, Yu X, et al. Co-occurrence of CDKN2A/B and IFN-I homozygous deletions correlates with an immunosuppressive phenotype and poor prognosis in lung adenocarcinoma. Mol Oncol 2022;16:1746–60.
39. Schwabe M, Brini AT, Bosco MC, Rubboli F, Egawa M, Zhao J, et al. Disruption by interferon-alpha of an autocrine interleukin-6 growth loop in IL-6-dependent U266 myeloma cells by homologous and heterologous down-regulation of the IL-6 receptor alpha- and beta-chains. J Clin Invest 1994;94:2317–25.
40. Baldini C, Danlos FX, Varga A, Texier M, Halse H, Mouraud S, et al. Safety, recommended dose, efficacy and immune correlates for nintedanib in combination with pembrolizumab in patients with advanced cancers. J Exp Clin Cancer Res 2022;41:217.
41. Schwartz LH, Litière S, de Vries E, Ford R, Gwyther S, Mandrekar S, et al. RECIST 1.1-update and clarification: from the RECIST committee. Eur J Cancer 2016;62:132–7.
42. Pitoiset F, Cassard L, El Soufi K, Boselli L, Grivel J, Roux A, et al. Deep phenotyping of immune cell populations by optimized and standardized flow cytometry analyses. Cytometry A 2018;93:793–802.
43. Love MI, Soneson C, Patro R. Swimming downstream: statistical analysis of differential transcript usage following Salmon quantification. F1000Res. 2018;7:952.
44. Köster J, Rahmann S. Snakemake-a scalable bioinformatics workflow engine. Bioinformatics 2018;34:3600.
45. Ewels P, Magnusson M, Lundin S, Käller M. MultiQC: summarize analysis results for multiple tools and samples in a single report. Bioinformatics 2016;32:3047–8.
46. Patro R, Duggal G, Love MI, Irizarry RA, Kingsford C. Salmon provides fast and bias-aware quantification of transcript expression. Nat Methods 2017;14:417–9.
47. Love MI, Huber W, Anders S. Moderated estimation of fold change and dispersion for RNA-seq data with DESeq2. Genome Biol 2014;15:550.
48. Sturm G, Finotello F, Petitprez F, Zhang JD, Baumbach J, Fridman WH, et al. Comprehensive evaluation of transcriptome-based cell-type quantification methods for immuno-oncology. Bioinformatics 2019;35:i436–45.
49. Yu G, Wang LG, Han Y, He QY. clusterProfiler: an R package for comparing biological themes among gene clusters. OMICS 2012;16:284–7.
50. Li H, Durbin R. Fast and accurate short read alignment with Burrows-Wheeler transform. Bioinformatics 2009;25:1754–60.
51. Van der Auwera GA, Carneiro MO, Hartl C, Poplin R, Del Angel G, Levy-Moonshine A, et al. From FastQ data to high confidence variant calls: the Genome Analysis Toolkit best practices pipeline. Curr Protoc Bioinformatics 2013;43:11.10.1–11.10.33.
52. DePristo MA, Banks E, Poplin R, Garimella KV, Maguire JR, Hartl C, et al. A framework for variation discovery and genotyping using next-generation DNA sequencing data. Nat Genet 2011;43:491–8.
53. Ramos AH, Lichtenstein L, Gupta M, Lawrence MS, Pugh TJ, Saksena G, et al. Oncotator: cancer variant annotation tool. Hum Mutat 2015;36:E2423–2429.
54. Li H, Handsaker B, Wysoker A, Fennell T, Ruan J, Homer N, et al. The sequence Alignment/map format and SAMtools. Bioinformatics 2009;25:2078–9.

55. Mayakonda A, Lin DC, Assenov Y, Plass C, Koeffler HP. Maftools: efficient and comprehensive analysis of somatic variants in cancer. Genome Res 2018;28:1747–56.
56. Merino DM, McShane LM, Fabrizio D, Funari V, Chen SJ, White JR, et al. Establishing guidelines to harmonize tumor mutational burden (TMB): in silico assessment of variation in TMB quantification across diagnostic platforms: phase I of the Friends of Cancer Research TMB Harmonization Project. J Immunother Cancer 2020;8:e000147.
57. Van Loo P, Nordgard SH, Lingjærde OC, Russnes HG, Rye IH, Sun W, et al. Allele-specific copy number analysis of tumors. Proc Natl Acad Sci U S A 2010;107:16910–5.